

Aus der
Neurochirurgischen Klinik und Poliklinik
Klinikum der Ludwig-Maximilians-Universität München



Investigating pericytes heterogeneity in glioblastoma vasculature

Dissertation
zum Erwerb des Doktorgrades der Medizin
an der Medizinischen Fakultät
der Ludwig-Maximilians-Universität München

vorgelegt von
Gen Li

aus
Jiaozuo / Henan

Jahr
2025

Mit Genehmigung der Medizinischen Fakultät der
Ludwig-Maximilians-Universität München

Erstes Gutachten: Prof. Dr. Rainer Glaß
Zweites Gutachten: Prof. Dr. Wolfgang Enard
Drittes Gutachten: Prof. Dr. Christoph Schmitz
weitere Gutachten:

Dekan: Prof. Dr. med. Thomas Gudermann

Tag der mündlichen Prüfung: 24.04.2025

Table of Contents

Table of contents	1
Zusammenfassung	5
Abstract	7
List of figures.....	9
List of tables.....	10
List of abbreviations	11
1. Introduction	13
1.1 Glioblastoma	13
1.2 Classification of glioblastoma	13
1.3 GBM recurrence	14
1.4 GBM Angiogenesis	16
1.5 Blood–brain barrier and blood–tumor barrier	17
1.5.1 Blood-brain barrier	17
1.5.2 Blood-tumor barrier.....	18
1.6 Pericytes.....	18
1.6.1 Pericytes in normal brain.....	18
1.6.2 Pericytes in glioblastoma.....	19
1.7 Vascular basement membrane, Lysyl oxidases family and β-aminopropionitrile (BAPN)	21
1.7.1 Vascular basement membrane	21
1.7.2 Lysyl oxidases family.....	21
1.7.3 β-aminopropionitrile (BAPN).....	22
1.8 Induced experimental GBM mice models	23
1.9 Objectives	24

2	Materials.....	25
2.1	Devices	25
2.2	Consumables	26
2.3	Cell culture materials	27
2.4	Reagents and chemicals.....	27
2.5	Primary antibodies	29
2.6	Secondary antibodies and other dyes	30
2.7	Streptavidin conjugates.....	31
2.8	Microscopy	31
2.9	Software.....	31
2.10	Mice strains	32
2.11	Vectors	32
3.	Methods	34
3.1	Cell Experiments.....	34
3.1.1	Cell culture	34
3.1.2	Neural precursor cells extraction and single cell suspension	34
3.1.3	Cell transfection.....	35
3.2	Animal experiments.....	35
3.2.1	Animal care	35
3.2.2	Tumor inoculation.....	35
3.2.3	Adeno-associated viruses application	36
3.2.4	Survival curve	37
3.2.5	Evans blue assay	37
3.2.6	Dextran leakage analysis	38
3.3	Histology	39

3.3.1	Perfusion and tissue preparation	39
3.3.2	Haematoxylin & Eosin (H&E) staining.....	40
3.3.3	Quantification of tumor volume.....	40
3.4	Immunofluorescence staining.....	41
3.4.1	Mice brain immunostaining process.....	41
3.4.2	Quantification of tumor angiogenesis (microvascular pattern)	41
3.5	3D reconstruction of tumor vessels	42
3.5.1	Tissue clearing and staining	42
3.5.2	Imaging and reconstruction.....	43
3.6	Statistics.....	43
4.	Results.....	45
4.1	Pericyte heterogeneity in glioblastoma	45
4.1.1	Lineage-tracing mice GBM models recapitulating different human GBM subtypes.....	45
4.1.2	Tumor take check and survival analysis of lineage-tracing mice GBM models recapitulating different human GBM subtypes.....	46
4.1.3	Definitions of different tumor regions and origins of pericytes	49
4.1.4	Host and tumor equally generated pericytes in AAV-induced p53 ^{KO} /Pten ^{KO} /Nf1 ^{KO} GBM models.....	51
4.1.5	The host and tumor equally generated pericytes in orthotopically injected transgenic p53 ^{KO} /Pten ^{KO} /Nf1 ^{KO} GBM models.	54
4.1.6	The host and tumor equally generated pericytes in CDKN2aKO and p53 ^{KO} /Pten ^{KO} /Nf1 ^{KO} GBM models.....	56
4.1.7	Vasculature analysis of all GBM subtypes.	58
4.1.8	Tissue clearing of mice GBM samples and 3D-reconstruction of tumor vessel structure.....	62
4.2	Pericytes ablation could upregulate BTB permeability in recurrent GBM mice models.....	64

4.2.1	The induction of pericyte depleted relapse GBM mice models	64
4.2.2	Early stage pericytes ablation significantly opened BTB.....	67
4.2.3	Vasculature analysis of relapse GBM models.....	69
4.3	Full-time BAPN application increased BTB permeability in primary GBMs	71
4.3.1	Full-time BAPN treatment could suppress tumorigenesis.....	71
4.3.2	Full-time BAPN treatment up-regulated Evans blue leakiness in tumor parenchyma	73
4.3.3	Full-time BAPN treatment aggravated dextran leakiness in tumor parenchyma.....	75
4.3.4	Full-time BAPN treatment did not affect the angiogenesis in GBM...	76
5.	Discussion.....	79
	References.....	88
	Contributions	103
	Acknowledgements	104
	Affidavit	105
	List of Publications	106

Zusammenfassung

Die Blut-Hirn-Schranke (BHS) ist entscheidend für die Aufrechterhaltung der physiologischen Funktionen des zentralen Nervensystems (ZNS). Eine regional heterogene und aberrante vaskuläre Barriere, auch als Blut-Tumor-Schranke (BTS) bezeichnet, wird im Glioblastom (GBM) aufrechterhalten. Die BTS kann die klinische Behandlung von GBM beeinträchtigen, indem sie die intratumorale Ansammlung von blutbasierten Therapeutika verhindert. Perizyten tragen zur Integrität der BHS bei, und es wurde bereits vorgeschlagen, dass tumorabgeleitete vaskuläre Muralzellen die BTS initiieren. Der Beitrag endogener Perizyten zur Bildung der BTS wurde jedoch bislang nicht ausreichend untersucht. In dieser Studie nutzten wir die Abstammungsverfolgung in verschiedenen transgenen GBM-Mausmodellen, die unterschiedliche menschliche GBM-Subtypen nachbilden, um den Anteil von tumor- oder wirtabgeleiteten vaskulären Muralzellen an der neoplastischen Vaskulatur zu identifizieren und zu quantifizieren. Diese Modelle ermöglichen die Klassifizierung des Ursprungs der Muralzellen und zeigen einen signifikanten und stabilen Beitrag wirtabgeleiteter Perizyten zu den GBM-Gefäßen. Wir fanden, dass die vaskuläre Musterbildung bei GBMs mit unterschiedlichen Treibermutationen variiert. Der Wirt und der Tumor generierten gleichermaßen eine Population intratumoraler vaskulärer Muralzellen, ohne dass dies vom GBM-Subtyp abhängt. Vaskuläre Muralzellen, insbesondere Perizyten, können verschiedene Komponenten der Basalmembran (BM) synthetisieren und die Proliferation, Migration und Differenzierung von Endothelzellen (EZ) regulieren, die an der BM haften. Die Stabilität der BM wird durch die Quervernetzung der Matrixkomponenten durch Lysyl-Oxidasen (LOX) erreicht. Ein LOX-Inhibitor wurde angewendet, um diese Quervernetzung zu unterdrücken, die BM abzubauen, und es wurde eine signifikante Erhöhung der Permeabilität der BTS festgestellt. Es wurden Mausmodelle mit konditionaler Perizytenablation induziert, in die Rezidivtumorzellen implantiert wurden, um die Perizytenablation in rezidivierenden GBMs zu stimulieren. Es wurde festgestellt, dass eine frühzeitige Perizytenablation die Permeabilität der BTS signifikant erhöhen kann. Insgesamt legen diese Daten nahe, dass tumorparenchymale

Perizyten vielversprechende therapeutische Ziele für die Modulation der BTS und eine verbesserte GBM-Behandlung darstellen.

Abstract

The blood–brain barrier (BBB) is essential for the maintenance of central nervous system (CNS) physiology. A regionally heterogeneous and aberrant vascular barrier (blood–tumor barrier [BTB]) is maintained in glioblastoma (GBM). The BTB can deteriorate clinical care for GBM by preventing the intratumoral accumulation of bloodborne therapeutics. Pericytes maintain the BBB integrity, and it has been previously proposed that tumor-derived vascular mural cells initiate the BTB. However, the contribution of endogenous pericytes to BTB formation has not been sufficiently explored. Here, the lineage-tracing capacity of a range of transgenic GBM mouse models were leveraged, recapitulating distinct human GBM subtypes, to identify and quantify the contribution of tumor- or host-derived vascular mural cells to the neoplastic vasculature. These models allow the classification of the mural cell origin and reveal a profound and stable contribution of host-derived pericytes to GBM vessels.[1] This research found that vascular patterning varied among GBM with different driver mutations. And the host and tumor equally generated a population of intratumoral vascular mural cells, without any dependence on the GBM subtype. Vascular mural cells, especially pericytes, could synthesize various basement membrane (BM) components and regulate the proliferation, migration, and differentiation of endothelial cells (ECs) which adhere to the BM. Stability of the BM is achieved through crosslinking of matrix components by lysyl oxidases (LOX). A LOX inhibitor was applied to suppress the crosslinking to breakdown the BM and found the permeability of BTB was significantly augmented. Conditional pericytes ablation

mouse models were induced, implanted with relapse tumor cells to stimulate the pericytes ablation in relapse GBMs. It was found that early pericyte ablation could significantly increase the permeability of the BTB. Overall, these data suggest that tumor parenchymal pericytes are therapeutically promising targets for BTB modulation and improved GBM treatment.

- [1] **Gen Li**, Jerry Voncken, Huabin Zhang, Dongxu Zhao, Roland E. Kälin and Rainer Glass. *Tracing pericyte heterogeneity in the glioblastoma vasculature*. Poster, Brain Tumor Meeting 2024, Berlin, Germany.

List of figures

Fig 1 Lineage-tracing mice GBM models recapitulating different human GBM subtypes.....	46
Fig 2 Tumor take check and survival analysis of lineage-tracing mice GBM models recapitulating different human GBM subtypes.....	48
Fig 3 Definitions of different tumor regions and origins of pericytes	50
Fig 4 PDGFB overexpression upregulated pericyte coverage in AAV-induced p53KO/PtenKO/Nf1KO GBM models.....	53
Fig 5 Host and tumor equally generated pericytes in orthotopically injected transgenic p53KO/PtenKO/Nf1KO GBM models.....	55
Fig 6 Host and tumor equally generated pericytes in CDKN2aKO, p53KO/PtenKO/Nf1KO GBM models.....	57
Fig 7 Vasculature analysis of all GBM subtypes.....	60
Fig 8 Tissue clearing of mice GBM samples and 3D-reconstruction of tumor vessel structure.....	63
Fig 9 Pericyte conditionally depleted relapse GBM models induction	66
Fig 10 Early stage pericytes ablation significantly opened BTB	68
Fig 11 Vasculature analysis of relapse GBM models.....	70
Fig 12 Full-time BAPN treatment could suppress tumorigenesis	72
Fig 13 Full-time BAPN treatment up-regulated Evans blue leakiness in tumor parenchyma	74
Fig 14 Full-time BAPN treatment aggravated dextran leakiness in tumor parenchyma.....	76
Fig 15 Full-time BAPN treatment did not obviously affect the angiogenesis in glioblastoma.	77

List of Tables

Table 2.1 Devices	25
Table 2.2 Consumables	26
Table 2.3 Cell culture materials.....	27
Table 2.4 Reagents and chemicals	28
Table 2.5 Primary antibodies.....	30
Table 2.6 Secondary antibodies and other dyes	30
Table 2.7 Streptavidin conjugates	30
Table 2.8 Microscopy	31
Table 2.9 Software	31
Table 2.10 Purchased mice for crossbreeding.....	32
Table 2.11 Mice used in present research.....	33
Table 2.12 Vectors.....	33

List of abbreviations

CNS	Central nervous system
GBM	Glioblastoma
IDH 1	Isocitrate dehydrogenase 1
EGFR	Epidermal growth factor receptor
PTEN	Phosphatase and tensin homolog
CDKN2A	Cyclin-dependent kinase inhibitor 2A
NF1	Neurofibromatosis type 1
TP53	Tumor protein 53
PDGFRA	Platelet-derived growth factor receptor- α
PDGFRB	Platelet-derived growth factor receptor- β
PDGFA	Platelet-derived growth factor A
PDGFB	Platelet-derived growth factor B
HIF-1	Hypoxia-inducible factor-1
VEGF	Vascular endothelial growth factor
EGF	Epidermal growth factor
FGF	Fibroblast growth factor
ECM	Extracellular matrix
MMPs	Metalloproteinases
EC	Endothelial cell

BBB	Blood-brain barrier
BTB	Blood-tumor barrier
LOX	Lysyl oxidases
BAPN	β -aminopropionitrile
SVZ	Subventricular zone
AAV	Adeno-associated virus
PBS	Phosphate-buffered saline
DFM	Dimethylformamide
PFA	Paraformaldehyde
vWF	von Willebrand factor
iDTA	Inducible diphtheria toxin A
DMEM	Dulbecco's Modified Eagle Medium
FBS	Foetal bovine serum
NPC	Neural precursor cell
GSC	Glioblastoma stem cells
FACS	Fluorescent activated cell sorting
FITC	Fluorescein-isothiocyanate
HSVTK	Herpes simplex virus tyrosine kinases
EB	Evans blue
i.p.	Intraperitoneal injection

1. Introduction

1.1 Glioblastoma

Gliomas are the most common intracranial malignancies in adults[1, 2]. The fifth edition of the World Health Organization's (WHO's) central nervous system (CNS) tumor classification graded glioblastoma as Grade IV, indicating high malignancy based on clinical, genetic, and histopathological features[3]. Glioblastoma (GBM), categorised as Grade IV as per the WHO standard, is the most common and aggressive primary intracranial tumor. It constitutes approximately 49% of malignant brain tumors and around 56% of all gliomas[2, 4]. GBM has an extremely poor prognosis, with a median survival of 14 to 16 months, despite modern multimodal therapies, including surgery combined with radiation and/or chemotherapy, sometimes also biological therapy[2, 5, 6]. Less than 10% of patients survive longer than 5 years[7].

1.2 Classification of glioblastoma

WHO classified GBM into two general subtypes: primary and secondary GBM [3]. Primary GBM accounts for approximately 90% of all GBM cases and is characterized by rapid development and non-association with isocitrate dehydrogenase 1 (IDH 1) gene mutation[8]. The remaining 10% of cases comprise secondary GBM, developed from low-grade (WHO II or III) astrocytoma and carry IDH 1 mutation[9]. Secondary GBM patients are usually younger than primary GBM, also have a better prognosis[10, 11].

Recent research has demonstrated that GBM cells have high heterogeneity, GBM cells

can be defined as neural progenitor-like, oligodendrocyte-like, astrocyte-like, and mesenchymal-like, based on combined bulk sequencing using The Cancer Genome Atlas (TCGA) database and single-cell sequencing (RNAseq)[12], this demonstrated that glioblastoma can be classified into three different subtypes named classical, mesenchymal and proneural subtypes[13]. The Classical subtype is characterized by increased expression of the epidermal growth factor receptor (*EGFR*), while bearing a loss of phosphatase and tensin homolog (*PTEN*) and cyclin-dependent kinase inhibitor 2A (*CDKN2A*) [14]. The classical subtype is also found responsive to radiotherapy and chemotherapy[15]. The signature genetic alterations of mesenchymal GBM harbor deletion of Neurofibromatosis type 1 (*NF1*), tumor protein 53 (*TP53*) and *PTEN*[16, 17]. This GBM subtype is also indicated associated with worse prognosis[18]. The proneural subtypes is characterized by overexpression of genes such as platelet-derived growth factor receptor- α (*PDGFRA*)[19]. An additional subtype, known as the Neural subtype, was previously included in the classifications. However, it is no longer considered a genuine GBM subtype. This change is due to findings that the neural subtype was likely an artifact resulting from contamination with normal parenchymal cells[20].

1.3 GBM recurrence

Conventional therapy for newly diagnosed GBM includes maximal safe surgical resection combined with radiation, temozolomide chemotherapy, and other treatments such as immunotherapy and tumor-treating fields [7]. However, even with first-line

multimodal treatment, most patients would still develop fatal recurrent tumors [21-23]. Recurrent GBM (rGBM) often occur close to the initial tumor site (mostly <2 cm from the primary lesion) and less frequent at distant sites, which can be associated with unifocal/multifocal parenchymal lesions or leptomeningeal spread [24, 25]. Because total resection of the primary malignancy is virtually impossible, researchers believe that the tumor cells left in the brain parenchyma are the origin of relapsing tumors. Unfortunately, once tumors relapse after standard care, the treatment options are limited. Less than 50% of rGBM patients are eligible for a second surgery (12–48%) [26-28], re-radiation only produces a modest clinical benefit compared to best supportive care alone [29], and several chemotherapeutic substances or tumor-treating fields have been proven to have limited or no efficacy in randomised trial settings [30-32]. Recently, other therapeutic methods have been tested in clinical trials, such as regorafenib, a tyrosine kinase inhibitor [33] and anti-angiogenic therapies, such as bevacizumab [34] and anlotinib [35, 36], but failed to show considerable improvement in outcome or were only effective in rare cases.

In our lab's previous research using murine primary tumor models, we found that interventions performed in the early stage of the GBM process suppressed tumorigenesis and tumor angiogenesis [37]. However, the difficulty of diagnosing early-stage primary GBMs makes it impossible to begin treatment at the beginning of the tumor process, relapse was induced in GBM models in this study to investigate whether rGBM could be terminated when treatment was applied at the early recurrent stage.

1.4 GBM Angiogenesis

GBM is a highly vascular brain tumor [38] and several angiogenic factors and receptors are involved in its vascularization and tumor growth[39]. The angiogenesis in GBM is initialised through the following steps: (1) hypoxia-induced angiogenic factor secretion, (2) migration and proliferation of endothelial cells (ECs) stimulated by angiogenic factors (3) the stabilization of newly generated vessels by mural cells[40, 41]. Hypoxia is considered the main trigger for activation of the transcription factor hypoxia-inducible factor-1 (HIF-1), which regulates the expression of growth factors[42], matrix components[43], adhesion molecules[44] and metabolic proteins[45]. The lack of oxygen promotes the release of pro-angiogenic proteins, including vascular endothelial growth factor (VEGF)[46], transforming growth factor- β (TGF- β)[47], fibroblast growth factor (FGFs)[48], angiopoietin-1[49] and epidermal growth factor (EGF)[50]. These proangiogenic proteins can bind to their related receptors on EC membranes to initiate migration and proliferation. These factors can cause vessel wall dissolution, basement membrane and extracellular matrix (ECM) degradation. Proteases, such as matrix metalloproteinases (MMPs) and stromal cells, can remodel the ECM and synthesise a new matrix, facilitating the migration and proliferation of ECs and resulting in the formation of endothelial tube-like structures[51]. Finally, mural cells, such as pericytes and smooth muscle cells, are recruited to cover the tube from the outside to stabilise the newly generated vessels[52, 53]. Since tumor angiogenesis supplies essential nutrients and oxygen to tumor cells, it is considered a therapeutic

target for GBM. However, most studies on anti-angiogenic treatment have failed to show a survival benefit for patients with GBM[54]. Bevacizumab, a monoclonal antibody approved by the United States Food and Drug Administration (FDA) to treat recurrent GBM[55] demonstrated a 2-month survival time increase when used in combination with conventional therapies[56]. However, this study did not find any improvement in overall mortality[56]. Furthermore, a range of antiangiogenic agents such as Cediranib and Imatinib also have been examined in different clinical trials, but no statistical significant improvement on overall survivals were observed[55]. Hence, there still exist significant challenges in the development of effective anti-angiogenic substances.

1.5 Blood–brain barrier and blood–tumor barrier

1.5.1 Blood–brain barrier

The blood–brain barrier (BBB) is a multicellular structure that regulates homeostasis and maintains normal CNS function[57]. The BBB contains ECs with tight junctions, pericytes (which are juxtaposed to ECs within the same basement membrane), and astrocytic endfeet [58]. The BBB controls the exchange of molecules between the CNS and peripheral nerves. It prevents a range of molecules, such as proteins, from freely crossing the blood compartment to the cerebral compartment [59, 60]. Essential nutrients are delivered through specific transport systems [61]. Macromolecules can use adsorptive-mediated transport (AMT) [62, 63], whereas small biomolecules such as glucose, amino acids, and hormones can cross the BBB via carrier-mediated transport

(CMT) [64-66] and highly selective and specific receptor-mediated transport (RMT) [67, 68]. Furthermore, toxins and metabolic molecules are excluded from the CNS to maintain the cerebral physiology [69].

1.5.2 Blood–tumor barrier (BTB)

In GBM the integrity of the BBB undergoes dramatic changes [64]. The pathological BBB in tumors is leakier than the normal BBB, and disruption can be revealed by magnetic resonance imaging (MRI) or positron emission tomography (PET) [70, 71]. The blood–tumor barrier (BTB) is characterised by aberrant pericyte coverage and loss of astrocytic endfeet or neuronal connections [72]. The BTB is heterogeneous and locoregionally may form intact barriers in tumors [73, 74]. The BTB is characterized e.g. through a range of efflux transporters that prevent the delivery of anticancer drugs [70, 71]. It is currently discussed in the field of neurooncology that in these low-permeability tumor regions, drugs cannot reach effective concentrations to kill tumor cells, ultimately enabling tumor relapse [75]. Generally, the BTB represents a central challenge for GBM therapy.

1.6 Pericytes

1.6.1 Pericytes in normal brain

Pericytes are embedded in the basement membrane of small vessels, including capillaries and pre- and post-capillary arterioles and venules [76-79]. It was demonstrated that pericytes play a vital role in maintaining CNS homeostasis. (1)

Pericytes regulate BBB permeability by controlling the expression and alignment of tight junction proteins and trans-barrier transport of different molecules [79-81]. Furthermore, interactions between ECs and pericytes can open a barrier for neuropharmaceutical delivery [82]. (2) Pericytes regulate angiogenesis, microvascular stability, and angioarchitecture during CNS development and vessel remodelling[76, 80, 83]. (3) Pericytes can clear tissue debris and foreign proteins out of the CNS [76, 80, 84, 85]. (4) Pericytes control capillary tone and diameter to regulate cerebral blood flow (CBF) [86, 87]. (5) Pericytes promote leukocyte adhesion and transmigration and influence neuroinflammation [88-90]. (6) Some researchers have found that pericytes have stem cell activity that enables them to differentiate into neural and vascular lineage cells under pathological conditions [91]. Pericyte dysfunction can cause BBB breakdown [81, 92, 93], aberrant angiogenesis [83, 84], neurotoxin accumulation [93, 94], CBF dysfunction [87, 88], immune dysregulation [89, 91] and compromised stem cell activity [92].

1.6.2 Pericytes in glioblastoma

Pericytes were previously considered to play an important role in maintaining CNS homeostasis in vessel structures. Recent studies have also elucidated their effects on disease [95, 96]. In GBM, pericytes play multifaceted roles such as promoting tumor initiation [95, 97]and invasion[98], regulating the BBB [97, 99] and tumor angiogenesis [100], and contributing to the immune microenvironment [101, 102]. Glioblastoma stem cells (GSCs), which assist in GBM cell proliferation, have been reported to

differentiate into pericytes in tumors [103]. Abnormal pericyte coverage on the BTB in GBMs allows tumor cells to spread to distant sites, and oedema within tumor tissue caused by low pericyte coverage can enhance tumor invasion by increasing the intratumoral fluid pressure [104, 105]. In addition, high intratumoral fluid pressure can suppress blood circulation and stimulate hypoxia to boost tumor invasion [106]. Moreover, abnormal pericyte coverage allows other solid tumors, such as lung cancer and melanomas, to migrate into the CNS, forming metastases [107, 108]. The BTB is considered a great challenge for drug delivery into GBMs, causing ineffective and nonuniform drug delivery [109, 110]. Tumor cells will not be exposed to effective concentrations of therapeutics and may relapse. Considering the functions of pericytes in regulating vessel permeability and stabilization, a huge effort has been made to halt the recruitment of pericytes by ECs and to open the BTB, in order to allow drugs to reach the tumor parenchyma [111, 112]. Pericytes play a vital role in tumor angiogenesis, especially in the interactions between pericytes and ECs. ECs were reported to secrete platelet-derived growth factor B (PDGFB) to recruit platelet-derived growth factor receptor β (PDGFRB) expressing pericytes that build a scaffold structure for ECs. In turn pericytes secrete vascular endothelial growth factor (VEGF) and angiopoietin-1 to stabilise the new vessels [113-115]. Interruption of this process e.g. through PDGFRB signalling in CNS development results in leaky vessels [116]. Furthermore, pericytes are involved in the stimulation of endothelial tip cells sprouting from exiting vessels in their vicinity, accelerating their proliferation and finally wrapping around ECs, resulting in vessel maturation [117].

In this study, PDGFRB conditional knockout mice models were used to investigate the BTB permeability when PDGFRB expressing cells were ablated from the barrier.

1.7 Vascular basement membrane, Lysyl oxidases family and β -aminopropionitrile (BAPN)

1.7.1 Vascular basement membrane

The basement membrane is an essential component of the BBB[118]. BM is a unique layer of ECM lies between endothelial cells, mainly consist of different ECM proteins such as collagens and elastin[119]. These ECM proteins were predominantly synthesised by endothelial cells and pericytes[119]. There are extensive interactions between these ECM proteins. Crosslinking, a crucial structural feature between elastin and collagens, provides flexibility to the vessels and maintains the integrity of the barrier[119]. And this crosslinking was found can be regulated by lysyl oxidases[120, 121].

1.7.2 Lysyl oxidase family

The lysyl oxidase family consists of lysyl oxidases (LOX) and four LOX-like (LOXL) isoforms [122]. They are involved in the cross-linking of collagen and elastin in the ECM of the basement membrane by catalysing the oxidation of lysines [120, 121]. These cross-links between collagen and elastin fibrils can provide structural integrity for collagen elastin sheets within the ECM and protect the matrix from degradation [123, 124]. LOXs are a range of hypoxia-regulated extracellular copper-dependent

enzymes [125], which have been demonstrated to be up-regulated in several cancers, such as breast [126-128], bladder [129], melanoma [130], lung [131-133], head and neck [134], and pancreatic [135, 136] tumors. In addition to its functions in maintaining ECM homeostasis, LOX has been found to facilitate tumor cell migration and promote metastasis [137]. These features of LOX make it a potential therapeutic target, and extensive research has been conducted to define its inhibitors to suppress its functions and treat tumors.

1.7.3 β -aminopropionitrile (BAPN)

β -Aminopropionitrile (BAPN) is a toxic constituent found in the peas of *Lathyrus* plants, for example, *Lathyrus odoratus* [138]. Ingestion of large quantities of BAPN will cause lathyrism, a disease known for centuries, encompassing two distinct entities: a disorder of the nervous system (neurolathyrism) leading to limb paralysis and a disorder of connective tissue, causing either bone deformity (osteolathyrism) or aortic aneurisms and dissections (andiolathyrism) [138, 139]. BAPN is widely used in animal experiments to induce aortic aneurysms and dissections because of its ability to dysregulate normal vessel formation [140]. Research has demonstrated that BAPN works as an inhibitor of LOX to break down the cross-linking of collagen and elastin within the ECM in the basement membrane, eventually disrupting normal vessel structure [125].

In this study, it was investigated whether BAPN can break down blood–tumor barrier formation in GBM to determine whether BAPN can be categorised as a potential

therapy to open the BTB to improve the effects of other substances.

1.8 Induced experimental GBM mouse models

To investigate the biology of GBM and to explore potential treatments, several types of GBM mouse models were used in laboratories, with distinct features and applications. The experimental GBM mouse models were generally separated into three different subtypes: syngeneic, xenograft and genetically engineered models. Syngeneic tumor cells were developed from murine host, the GL261 model is the first and most common used cell line, which could provide an intact tumor immune system[141]. Xenografted tumor cell lines were developed from human GBM multiforme, such as U87-MG[142], UM251-MG[143] and T98G[144]. Both syngeneic and xenografted GBM cell lines could be implanted in murine to induce experimental GBM models.

A variety of genetic mutations have been described in human glioblastoma, including these frequently disrupted cell-cycle and apoptosis regulation (*INK4a*, *CDK4*, *RB*, *TP53*), and growth factor signaling (*EGFR*, *PDGFR*, *PTEN*)[145]. A range of mouse models were exploited by introducing these oncogenic mutations into germline or specific cell subpopulations in brain to generate GBM models phenocopy human malignancies[146]. *TP53*, *NF1* and *Pten* genes were indicated among the top five mutated genes in human GBMs[147]. Mouse strains with germline or somatic mutations of *TP53*, *NF1* and *Pten* tumor suppressors were found to develop high-grade GBM with 100% penetrance[148, 149]. The subventricular zone (SVZ) is a layer on

the walls of lateral ventricles containing large amount of neural progenitor/precursor cells[150]. Recent research demonstrated that tumor suppressor floxed mice (*TP53^{flox/flox}*, *NF1^{flox/flox}* and *Pten^{flox/flox}*) injected with cre-recombinase encoding vectors into the SVZ induced GBM[146].

1.9 Objectives

The aims of this research are:

1. To investigate the heterogeneity of pericytes in primary GBM using transgenic mouse models recapitulating different genetic subtypes of human GBM.
2. To explore the role of the vascular basement membrane in BTB formation and the impact of matrix modulating agents in preventing BTB development.
3. To evaluate the function of endogenous pericytes in relapsing GBM using transgenic mouse models.

2. Materials

2.1 Devices

Table 2.1 Devices

Equipment	Company
Centrifuge	Thermo Fisher Scientific/Eppendorf
Clamp mount micromanipulators	AD Instruments
Countess II FL automated cell counter	Thermo Fisher Scientific
Digital vortex mixer	VWR
Fridge (4°C, -20°C)	Liebherr
Freezer (-80°C)	Thermo Fisher Scientific
Hera safe hood	Thermo Fisher Scientific
Incubator	Thermo Fisher Scientific
Magnetic hotplate stirrer	VWR
Microliter syringe	Hamilton
Micropipette (10 µL, 20 µL, 100 µL, 200 µL, 1000 µL)	Eppendorf
Microtome slide 2003	PFM medical AG
Microwave	Siemens
Mastercycler nexus gradient	Eppendorf
Perfusion system dose IT P910	Integra Biosciences AG
pH meter WTW multical bench	Sigma Aldrich
Pipette boy	Eppendorf

Shaker	Biozyme Scientific
Infinite® 200 PRO	Tecan
Stereotactic frame	Stereotactic Frame
Surgical instruments	Aesculap
Water bath	Memmert

2.2 Consumables

Table 2.2 Consumables

Product	Company	CatLog Number
Cell culture flask (T25)	TPP	90026
Cell culture flask (T50)	TPP	90076
Cell culture flask (T75)	TPP	90151
Centrifuge tubes (0.5 mL)	Eppendorf	0030121.023
Centrifuge tubes (1 mL)	Eppendorf	0030121.694
Centrifuge tubes (2 mL)	Eppendorf	0030121.094
Centrifuge tubes (15 mL)	TPP/Falcon	91015
Centrifuge tubes (50 mL)	TPP/Falcon	91051
Coverslip	Gerhard Menzel	9.160829
Ethicon excel (5–0) sutures	Ethicon	389065
Glass slides	Epredia	J1800AMNZ
Microtome blade A35	Feather	36-099-2334
Pap-pen	Dako	S2002

Pipette tips (10 μ L, 100 μ L, 200 μ L, 1000 μ L)	Eppendorf	3123000020/3123000047/3123000055/3123000063
6-well plate	TPP	Z707775
24-well plate	TPP	92424
Scalpel (#15)	Feather	504172
Syringe (1 mL)	Braun	9166017
Syringe needle (30G, 27G, 23G)	Braun	305400
Tissue-tek-cryomold (15 mm \times 15 mm \times 5 mm)	Sakura Finetek	25608-924

2.3 Cell culture materials

Table 2.3 Cell culture materials

Material	CatLog Number	Company
DMEM	FG0415	Biochrom
Foetal bovine serum	10270-106	Life Technologies
Penicillin-streptomycin	15140-122	Life Technologies
Trypan-blue Solution 0.4%	T8154	Sigma Aldrich
Trypsin/EDTA	L2153	Merck Millipore
F12	17504044	Thermo Fisher Scientific
B27	11320074	Thermo Fisher Scientific

2.4 Reagents and chemicals

Table 2.4 Reagents and chemicals

Product	Supplier	Catalog Number
Agarose	Sigma Aldrich	9012-36-6
Aqua	B. Braun Melsungen AG	67240920000
Aquatex mounting medium	DAKO	S3023
Bepanthen	Bayer	82290583
Citric acid monohydrate	Sigma Aldrich	77-92-9
DAPI	Fluka	32670
Donkey serum	Jackson ImmunoResearch	017-000-121
Dextran, biotin, 70,000 MW	Invitrogen	D1957
Dextran, fluorescein, 2,000,000 MW	Invitrogen	D7137
Evans Blue	Sigma	314-13-6
Eosin solution	Sigma Aldrich	15086-94-9
Ethanol 100%	Carl Roth	64-17-5
Ethanol 70%	Carl Roth	64-17-5
Ethanol 96%	Carl Roth	64-17-5
Ethylene glycol	Sigma Aldrich	107-21-1
Glycerol	Sigma Aldrich	56-81-5
HCl	Sigma Aldrich	7647-01-0
Haematoxylin	Roth	T865.2
Ketamine 10%	Zoetis Deutschland GmbH	4025270000

NaCl 0.9%	B. Braun Melsungen AG	69488220000
Paraformaldehyde (PFA)	Sigma Aldrich	30525-89-4
PBS	Apotheke Klinikum der Universität München	-
Pentobarbital (Narcofen®)	Merial	798-594
Povidone iodine solution 7.5%	B. Braun Melsungen AG	1588716
Protein block serum-free	Dako	X0909
Rompun 2%	Bayer	PZN-1320422
Roti® Histol	Carl Roth	6640.1
Sucrose	Sigma Aldrich	84100-250G
Tri-natriumcitrat-dihydrate	Sigma Aldrich	6132-04-03
Tris base	Sigma Aldrich	77-86-1
Triton X-100	Roche Diagnostics	93418
Tween-20	Sigma Aldrich	2001-0250
Urea	Sigma Aldrich	U-6478
N,N,N',N'-tetrakis (2- hydroxypropyl) ethylenediamine	Sigma Aldrich	122262
2,2',2''-nitrilotriethanol	Sigma Aldrich	90279
Triton X-100	Sigma Aldrich	T8787
Dimethylformamide (DMF)	Sigma Aldrich	227056

2.5 Primary antibodies

Table 2.5 Primary antibodies

Antigen	Host Species	Isotype	Dilution	Catalog number	Provider
von Willebrand Factor (vWF)	Rabbit	IgG	1:400	A0082	DAKO
CD31	Rat	IgG	1:50	550274	R&D
PDGFRB	Goat	IgG	1:200	AF1042	R&D

2.6 Secondary antibodies and other dyes**Table 2.6 Secondary antibodies and other dyes**

Conjugate	Antigen	Host Species	Dilution	Catalog number	Provider
Alexa fluor 488	Goat IgG	Donkey	1:500	705-545-147	Jackson Immuno Research
Alexa fluor 647	Rabbit IgG	Donkey	1:500	711-606-152	Jackson Immuno Research
Cy5	Rat IgG	Donkey	1:500	712-175-150	Jackson Immuno Research
Biotinylated	Goat IgG	Horse	1:200	BA9500	Vector
Biotinylated	Rabbit IgG	Donkey	1:200	711-065-152	Jackson Immuno Research

2.7 Streptavidin conjugates**Table 2.7 Streptavidin conjugates**

Conjugation	Dilution	Catalog number	Provider
Alexa fluor 488-streptavidin	1:500	016-540-084	Jackson

conjugate			ImmunoResearch
Alexa fluor 594-streptavidin conjugate	1:500	016-580-084	Jackson ImmunoResearch
Alexa fluor 647-streptavidin conjugate	1:500	016-600-084	Jackson ImmunoResearch

2.8 Microscopy

Table 2.8 Microscopy

Microscope	Supplier
Leica SP8X wll upright confocal microscope	Leica Microsystems
Leica DMI8 inverted confocal microscope	Leica Microsystems
Microscope axioskop 2	Carl Zeiss
Microscope axiovert 25	Carl Zeiss
Microscope camera axiocam	Carl Zeiss

2.9 Software

Table 2.9 Software

Software	Company
Axiovision rel. 4.8/4.9 software	Carl Zeiss
AngioTool software	NIH
LAS X software	Leica Microsystems
ImageJ	NIH
GraphPad Prism	GraphPad Software

IMARIS	Oxford Instruments
--------	--------------------

2.10 Mice strains

The information of mice purchased for crossbreeding was listed in Table 2.10. All multi-transgenic mice used in this research (listed in table 2.11) were crossbred by these purchased transgenic mice and housed in the animal room at the Walter Brendel Experimental Center, LMU. The genotypes of the mice were determined through genotyping.

Table 2.10 Purchased mice for crossbreeding

Mice strain	Strain number	Supplier
Ai9-tdTomato	007909	The Jackson laboratory
Cdkn2a ^{-/-}	01XBU	NCI-Frederick National Laboratory
p53KO	002101	The Jackson laboratory
pten ^{fllox}	006440	The Jackson laboratory
NF1 ^{fllox}	017639	The Jackson laboratory
PDGFRb-cre	029684	The Jackson laboratory
Rosa26-iDTA	009669	The Jackson laboratory

Table 2.11 Mice used in present research

Mouse Strains	Abbreviated as
p53 ^{fl/fl} , PTEN ^{fl/fl} , NF1 ^{fl/fl} , Ai9-tdTomato mice	P53/pten/nf1-flox

CDKN2aKO, p53 ^{fl/fl} , PTEN ^{fl/fl} , NF1 ^{fl/fl} , Ai9-tdTomato mice	CDKN2aKO
PDGFRB::CreERT2, Ai9-tdTomato mice	PDGFRB reporter
PDGFRB::CreERT2, R26 LSL diphtheria toxin subunit alpha (DTA), Ai9-tdTomato mice	PDGFRB-iDTA

2.11 Vectors

All vectors used in this research were designed by my group leader.

Table 2.12 Vectors

Adeno-associated viruses	Abbreviated as	Company
AAV1/2-CAG-NLS-cre-WPRE-MiniPolyA	AAV-cre	Sirion Biotech GmbH
AAV1/2-CAG-PDGFA-IRES-NLS-cre-WPRE-MiniPolyA	AAV-PDGFA	Sirion Biotech GmbH
AAV1/2-CAG-PDGFB-IRES-NLS-cre-WPRE-MiniPolyA	AAV-PDGFB	Sirion Biotech GmbH
Lentiviruses particles (include CAG-IRES-GFP-Cre)	/	GeneTarget Inc
Lentiviruses particles (include CAG-IRES-PDGFB-GFP-Cre)	/	GeneTarget Inc

3. Methods

3.1 Cell experiments

3.1.1 Cell culture

The mouse GBM cells GL261 were cultured under adherent conditions with Dulbecco's Modified Eagle Medium (DMEM) containing 1× MEM non-essential amino acids, 10% foetal bovine serum (FBS) and 1% penicillin (100 units/mL)–streptomycin (100 ug/mL). Floating cells were cultured in DMEM-F12 medium containing 1× B27, 10 ng/mL human EGF, 10 ng/mL human fibroblast growth factor (hFGF), 1% penicillin (100 units/mL)–streptomycin (100 µg/mL). The culture medium was changed twice or thrice per week based on the cell growth conditions. GL261 cells were passaged using trypsin when 70% of the flask space was occupied. Floating cells were split using Accutase when large spheres were formed. All cells were maintained in a 37 °C humidified incubator with 5% CO₂ atmosphere.

3.1.2 Neural precursor cells extraction and single cell suspension

Neural precursor cells (NPCs) were extracted from the subventricular zone (SVZ) of the p53^{fl/fl}/PTEN^{fl/fl}/NF1^{fl/fl} tdTomato mice. The mice were anaesthetised using Narcoren and sacrificed by cervical dislocation. The brain was removed and the SVZ tissue was collected. A surgical blade was used to cut the tissues into small pieces. The samples with 1× trypsin, to digest single cells. The treated cells were cultured in DMEM-F12 medium.

3.1.3 Cell transfection

The extracted single neural precursor cells (NPCs) were cultured in DMEM-F12 until large cell spheres floated on the medium. For transfection, cells were prepared as single cells and seeded at a density of 500,000 cells/2 mL per well in 6-well plates. Transfection was performed with lentiviruses containing CAG-IRES-GFP-Cre or CAG-IRES-PDGFB-GFP-Cre. After transfection, fluorescent activated cell sorting (FACS) was performed to sort transfected cells using tdTomato fluorescence.

3.2 Animal experiments

3.2.1 Animal care

All animal experiments were conducted according to the protocols of local authorities and the regulations of the National Guidelines for Animal Protection, Germany. All animals were kept in the Walter Brendel Experimental Centre with sufficient food and water *ad libitum* in standard cages in a cabinet with a 12-light and dark cycle. The mice were examined daily and sacrificed when they were symptomatic or at specific time points, depending on the experimental plan.

3.2.2 Tumor inoculation

Mice were intraperitoneally (i.p.) anaesthetised with mixed anaesthesia (0.36 mL 2% Rompun, 1.02 mL of 10% ketamine and 4.86 mL of normal saline) at a dosage of 7 μ L/g body weight. After the mice were anaesthetised, disinfection was performed on

the head with 7.5% povidone–iodine and Bepanthen® eye cream was applied. A midline incision was made on the skin of the head to expose the skull and stabilise the mouse in the stereotactic frame in the flat skull position. A skull puncture was gently made 1 mm anterior and 1.5 mm laterally to bregma. Next, the 1 µL Hamilton micro syringe was rinsed thoroughly with decreasing concentrations of ethanol (99%, 96%, 70% and 50%), aqua and 1× PBS, then taking tumor cells. Tumor cells were prepared at a density of 100,000 cells/µL in culture medium, and 1 µL of cells were injected into each mouse at a depth of 3 mm under the skull inner surface within 2 min. After all the cells were successfully injected, the syringe was carefully removed within 3 min, and the skin was sutured.

3.2.3 Adeno-associated viruses application

Adeno-associated viruses (AAVs) were designed by our lab and purchased from the Sirion Company. Mice were intraperitoneally (i.p.) anaesthetised with a mixed anaesthetic (0.36 mL of 2% Rompun, 1.02 mL of 10% ketamine and 4.86 mL of normal saline), at a dosage of 7 µL/g body weight. Next, disinfected head skin with 7.5% povidone–iodine and Bepanthen® eye cream was applied. A 10 µL Hamilton micro syringe was rinsed thoroughly with decreasing concentrations of ethanol (99%, 96%, 70%, and 50%), aqua and 1× PBS, and subsequently fixed on the micropump to take up the demanded volume of AAVs. The mouse was fixed on a stereotactic frame in the flat skull position. A midline incision was made on the head skin, and the mouse was stabilised on a stereotactic frame in the flat skull position. Several injection coordinates

were tested through pre-experiments to screen out the most effective virus implantation site. The most effective coordinates were adopted and demonstrated as follow. A skull puncture was gently made 1 mm anterior and 0.8-1.0 mm laterally to bregma. The micro syringe was inserted into the brain through the drilled hole to 2.5 mm depth, followed by withdrawing 1 mm, and injecting 1 μ L of AAV within 5 min (0.2 μ L/min). The needle was slowly withdrawn within 3 min, and the hole drilled in the skull was blocked with dental cement. After the cement dried, the mice's skin was sutured.

3.2.4 Survival curve

The survival time of all experimental mice was recorded using GraphPad PRISM 9.0, and a Kaplan–Meier survival curve was generated to demonstrate the correlation between each group. The relationship was tested by log-rank test, $P < 0.05$ was considered significant.

3.2.5 Evans blue assay

Evans blue (EB) powder was dissolved in a 0.9% NaCl solution at 2% concentration (2 g in 100 mL) and stored at room temperature. Mice were anaesthetised intraperitoneally with mixed anaesthesia (0.36 mL 2% Rompun, 1.02 mL of 10% ketamine and 4.86 mL of normal saline) at a dosage of 7 μ L/g body weight and stabilised in a tail vein injection tube. Ethanol (70%) was used to disinfect the skin and to widen the veins on both sides of the tail. Next, 2% Evans blue solution was taken with a 1 mL syringe equipped with a 30G needle; 200 μ L Evans blue solution was injected through the tail vein. EB was

maintained in the mouse circulation for 15 min. Then EB injected mice were anesthetised with Nacoren and stabilised on a perfusion table, a cut was made on the right atrial appendage and insert the perfusion needle into left heart ventricle from the heart tip. Mice were perfused at 8.7 mL/min speed with 10 mL of 1 PBS to wash out the EB in vessel lumens. The brain was removed, the cerebellum and brain stem were discarded, the brain was divided into two hemispheres (tumor-bearing and tumor-free), and the weights of the samples were recorded. The samples were homogenised with dimethylformamide (DFM) (2.67 μ L per gram brain tissue) and incubated the homogenate in a 37°C incubator overnight. On the second day, the samples were centrifuged at 16,000 \times g for 40 min and the supernatant was collected. Next, 100 μ L of the supernatant was added to one well on a 256-well plate and scanned with a Tecan reader to measure the absorbance at 620 nm. The absorbance was measured at 620 nm using a standard formula (calculated using different concentrations of EB solutions) to calculate the EB leakiness volume. Results were normalised to the average tumor volume of each model.

3.2.6 Dextran leakage analysis

70kDa biotin-related fixable dextran or 2000kDa fluorescein–isothiocyanate (FITC)-dextran was injected through the tail vein of mice, and the injected mice were perfused with 4% PFA solution to fix the dextran. Mouse brains were collected and kept in 4% PFA solution overnight for fixation, followed by 2 to 3 days of 30% sucrose dehydration. Frozen brains were cut into 40 μ m horizontal slices. After immunostaining, brain slices

were inspected using confocal laser scanning microscopy (TCS SP8, Leica) and images were obtained. All images were acquired at identical laser powers and processed using the same thresholds.

For the quantification of dextran, at least nine pics (40× magnification) were used for each mouse, and the analysis was performed using ImageJ software. Leakage of dextran into the tumor parenchyma was calculated by subtracting the amount of dextran inside the endothelial cells and vessel lumen.

3.3 Histology

3.3.1 Perfusion and tissue preparation

Mice were anaesthetised with Nacoren before sacrifice, fixed on a perfusion table, the chest skin was disinfected, and the chest was opened gradually to expose the whole heart. An incision was made in the right atrial appendage, and a perfusion needle was inserted into the left heart ventricle from the heart tip. Mice were perfused at 8.7 mL/min speed with 10 mL of 1× PBS, 15 mL of 4% PFA and 10 mL of 1× PBS × turn. The brain was taken out carefully, and the sample was kept in 4% PFA at 4°C overnight for post-fixation. Next, PFA was changed to 30% sucrose and stored at 4°C for 2 to 3 days to dehydrate to osmotic pressure. The brains were subsequently embedded in cryomatrix and frozen in liquid nitrogen. The brains were cut into 40 µm sections using a microtome or 200 µm sections by vibratome and stored in cryoprotective liquid (25% glycerol, 25% ethylene glycol and 50% 1×PBS) for later use.

3.3.2 Haematoxylin & Eosin (H&E) staining

The brain slices of interest were mounted on glass slides and air-dried. The staining was performed in glasswares as per the following steps: (1) immerse slides in 100% ethanol for 30 s for dehydration, (2) transfer the slides into haematoxylin solution for 2 min to dye the nucleus, (3) wash the slides with running distilled water for 5 min, (4) transfer the slides into eosin solution and immerse for 30 s for cytoplasm staining, (5) briefly rinse the slides with distilled water for washing, (6) transfer the slides into different concentrations of ethanol (20 s in 70%, 1 min in 96%, 1 min in 100%) for dehydration, (7) rinse the slides in Roti Histol for 1 min, (8) mount EntellanTM medium on the slides and cover with coverslips, let the slides air dried inside hood overnight, (9) image the prepared slides using the Carl Zeiss Axioskop 2 system with Axiovision Rel. 9.4 software.

3.3.3 Quantification of tumor volume

The quantification of tumor volume was performed as follows: (1) 10 transverse layers (horizontal sections) of mice brain slices were found out: $z = -1.24$ mm, -1.68 mm, -2.04 mm, -2.56 mm, -2.96 mm, -3.28 mm, -3.60 mm, -4.12 mm, -4.56 mm, and -5.04 mm (distance to inner surface of the skull), (2) H&E staining was performed, and images were acquired with the AxioVision software (Carl Zeiss), $1.5\times$ objective was used, (3) the tumor area (mm^2) of each section was calculated and the total area (mm^2) was summed up, (4) the average area was calculated as follows: $A_{\text{average}} (\text{mm}^2) = A_{\text{total}} / \text{number of consecutive sections with tumor}$, (5) stereotactic coordinates of the first

section (Z_{first}) and last section (Z_{last}) were checked taking tumor, and the height was calculated: $H_{\text{tumor}} = Z_{\text{last}} - Z_{\text{first}}$, (6) the tumor volume was calculated using the following formula: $V_{\text{tumor}} (\text{mm}^3) = A_{\text{average}} * H_{\text{tumor}}$.

3.4 Immunofluorescence staining

3.4.1 Mice brain immunostaining process

Brain slices of interest were selected from cryoprotective liquid, washed thrice with PBST (1×PBS containing 0.1% Tween20) placed in 12-well plates for 5 min each time, thrice in total. The washed brain slices were next immersed in 10% donkey serum in PBST (1×PBS containing 0.3% Triton X-100) for 30 min at room temperature to block nonspecific antigens. After blocking, the brain slices were transferred to primary antibody solutions and incubated at 4°C overnight. On the second day, the samples were washed with washing buffer for 5 min, three times, before being transferred to a secondary antibody solution. For secondary antibody staining, 2 h long light protected incubation at room temperature was performed, followed by washing steps as described previously. The slices were then mounted on glass slides, air-dried (approximately 15 min), stained with DAPI for 5 min, rinsed with distilled water, and air-dried. Finally, the slides were mounted with a fluorescence mounting medium and covered with a coverslip. The slides were kept in a dark and dry place at least overnight to dry the slides.

3.4.2 Quantification of tumor angiogenesis (microvascular pattern)

The AngioTool software was used to analyse the tumor vasculature by CD31/vWF staining to reveal tumor angiogenesis in all experimental groups. Images (20× magnification) were obtained for analysis by confocal microscopy. Several morphometric parameters, including vessel area, vessel density, total number of junctions, total vessel length, and average vessel length, were used to assess tumor angiogenesis. Each parameter was defined as follows:

- (1) Vessel area: the area of segmented vessels,
- (2) Vessel density: the percentage of area occupied by vessels,
- (3) Total number of junctions: the total number of vessel junctions in the image,
- (4) Total vessel length: sum of the Euclidean distances between the pixels of all vessels in the image.
- (5) Average vessel length: mean length of all the vessels in the image.

3.5 3D reconstruction of tumor vessels

3.5.1 Tissue clearing and staining

2000kDa FITC-dextran was injected into the tail vein before sacrifice to mark the vessel lumens. After cardiological fixation with 4% PFA, brain samples were collected and fixed with 4% PFA, followed by 30% sucrose. Frozen brains were cut into 200 μm horizontal slices and stored in cryoprotective liquid. Samples of interest were selected and washed in 1×PBS, cultured with shaking in a 37°C incubator with Reagent-1 (25wt% urea and 25wt% *N,N,N',N'*-tetrakis (2-hydroxypropyl), ethylenediamine was stirred to dissolve in distilled water in a 40°C water bath. Afterward, 15wt% Triton X-100 was

added for 72 h) [151]. After washed with PBST (Tween 20) 6 h × 3 times, the samples were transferred to PDGFRB staining for 48 h at room temperature, followed by washing step and related secondary antibody staining for 48 h at room temperature. Reagent-2 (50wt% sucrose, 25wt% urea and 10wt% 2,2',2''-nitrioltriethanol were stirred to dissolve in distilled water in a 40°C water bath, Triton X-100 was added as the last step) culturing was performed on a shaker in a 37°C incubator for 72 h, and the samples were washed with PBST (Tween 20) 6 h × 3 times [151]. The prepared tissues were kept in 30% sucrose solution at -20°C fridge until imaging.

3.5.2 Imaging and reconstruction

The tissues were washed with 1×PBS, mounted on glass slides, and covered with coverslips using a fluorescence mounting medium. After the slides were air-dried, confocal laser microscopy was used to capture Z-stack images (40× magnification). The T-stack raw file was transformed into an IMARIS-file file using an IMARIS file converter and run on IMARIS. The surface mode was used to reconstruct the three-dimensional (3D) structures of endothelial cells, endogenous pericytes, and tumor-derived pericytes. High-magnification 3D images were obtained to show detailed vessel structures.

3.6 Statistics

All statistical analyses were performed using the GraphPad Prism 9.0 software (GraphPad Software, Inc. CA. USA). The statistical significance of the survival curve

was calculated using the log-rank method. Differences between two groups were calculated using Student's *t*-test, and differences between more than two groups were examined using one-way analysis of variance (ANOVA). *P*-value was set less than or equals < 0.05 and was considered significant.

4. Results

4.1 Pericyte heterogeneity in glioblastoma

4.1.1 Lineage-tracing mice GBM models recapitulating different human GBM subtypes

In this study, the lineage-tracing capacity of a range of transgenic GBM mouse models were leveraged, recapitulating distinct human GBM subtypes, including AAV-induced GBM mouse models and orthotopically injected transgenic glioblastoma cell-induced GBM models. The AAVs (AAV1/2-cre, AAV1/2-PDGFA-cre and AAV1/2-PDGFB-cre) were injected into the subventricular zone (SVZ) in $p53^{fl/fl}/PTEN^{fl/fl}/NF1^{fl/fl}$, tdTomato mice and CDKN2aKO, $p53^{fl/fl}/PTEN^{fl/fl}/NF1^{fl/fl}$, tdTomato mice to transfect neural precursor cells (NPCs) and depleted tumor suppressors and induce spontaneous GBMs (Fig 1A). Transgenic GBM cells (GSCs) were generated by transfecting NPCs extracted from the SVZ of $p53^{fl/fl}/PTEN^{fl/fl}/NF1^{fl/fl}$ tdTomato mice. They were next implanted into mouse brains (100,000 cells/mouse) to induce GBMs (Fig 1B).

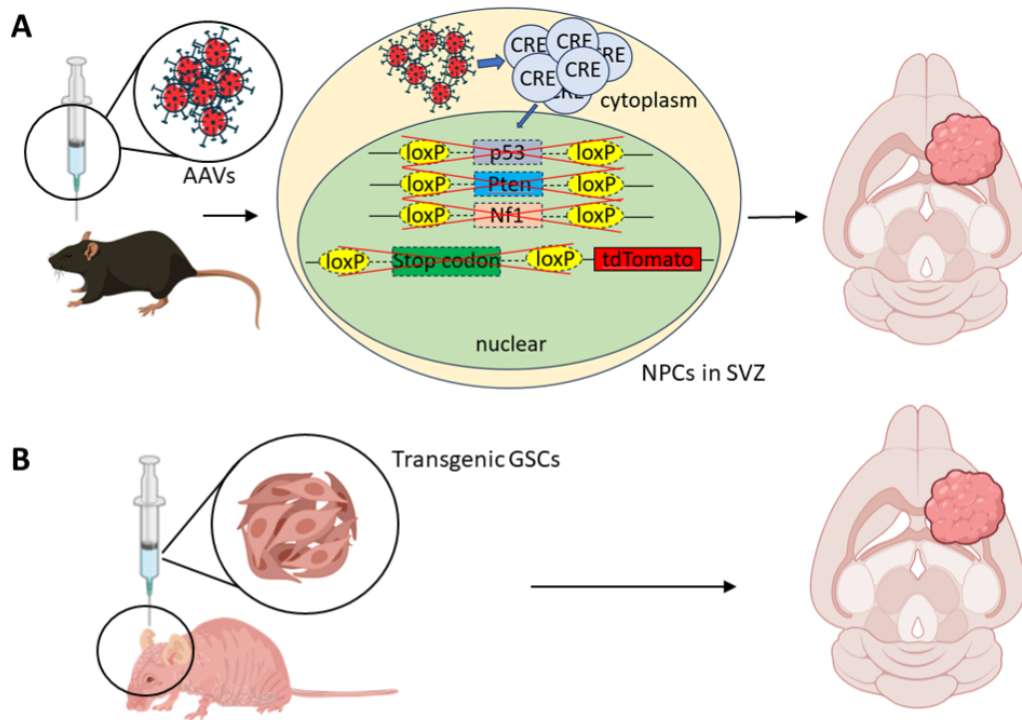


Figure 1 | Lineage-tracing mice GBM models recapitulating different human GBM subtypes

(A) Schematic diagram of the induction of transgenic lineage tracing GBM mice models by AAVs. AAVs were injected to mice SVZs to achieve the deletions of tumor suppressors, eventually develop into GBMs. (B) Schematic diagram of the induction of transgenic lineage tracing GBM models by orthotopic implantation of transgenic GBM cells. Transgenic tumor cells were injected into mice brains to develop GBM mice models.

4.1.2 Tumor take check and survival analysis of lineage-tracing mice GBM models recapitulating different human GBM subtypes

As described previously the induction of lineage-tracing GBM models, all mice models

were sacrificed when mice became symptomatic and brain samples were collected. H&E staining and immunostaining were performed to check the tumor uptake. Representative H&E staining and immunostaining images of AAV induced p53/Pten/Nf1 KO mice models (Fig 2A), orthotopically implanted transgenic GBM models (Fig 2B) and AAV induced Cdkn2aKO models were shown (Fig 2C). The GBMs were successfully induced (circled with white dotted line in both H&E staining and immunostaining). In H&E staining, and immunostainings, tumor cells were unevenly distributed in tumor region. In H&E staining, tumor cell nuclei with high DNA content were stained dark purple by hematoxylin, while abnormal cytoplasmic components and extracellular structures were stained pink by eosin. The necrotic areas appeared light color inside of tumor regions. In immunostainings, the lineage-tracing GBM models allow tdTomato positive tumors to be observed. A survival curve was drawn to compare the survival time of GBM models with different genotypes (Fig 2D). The result show, in different AAVs induced p53^{KO}/Pten^{KO}/Nf1^{KO} GBM models, that PDGFB overexpression significantly shortens the survival time compared to non-overexpression controls and PDGFA overexpression. Meanwhile, PDGFA overexpression significantly shortens the survival time as compared to non-overexpression controls. But in orthotopically implanted transgenic tumor models, PDGFB overexpression showed longer survival time than non-overexpression controls. Moreover, in different AAVs induced Cdkn2aKO models, PDGFB overexpression significantly reduced the survival time as compared to PDGFA overexpression.

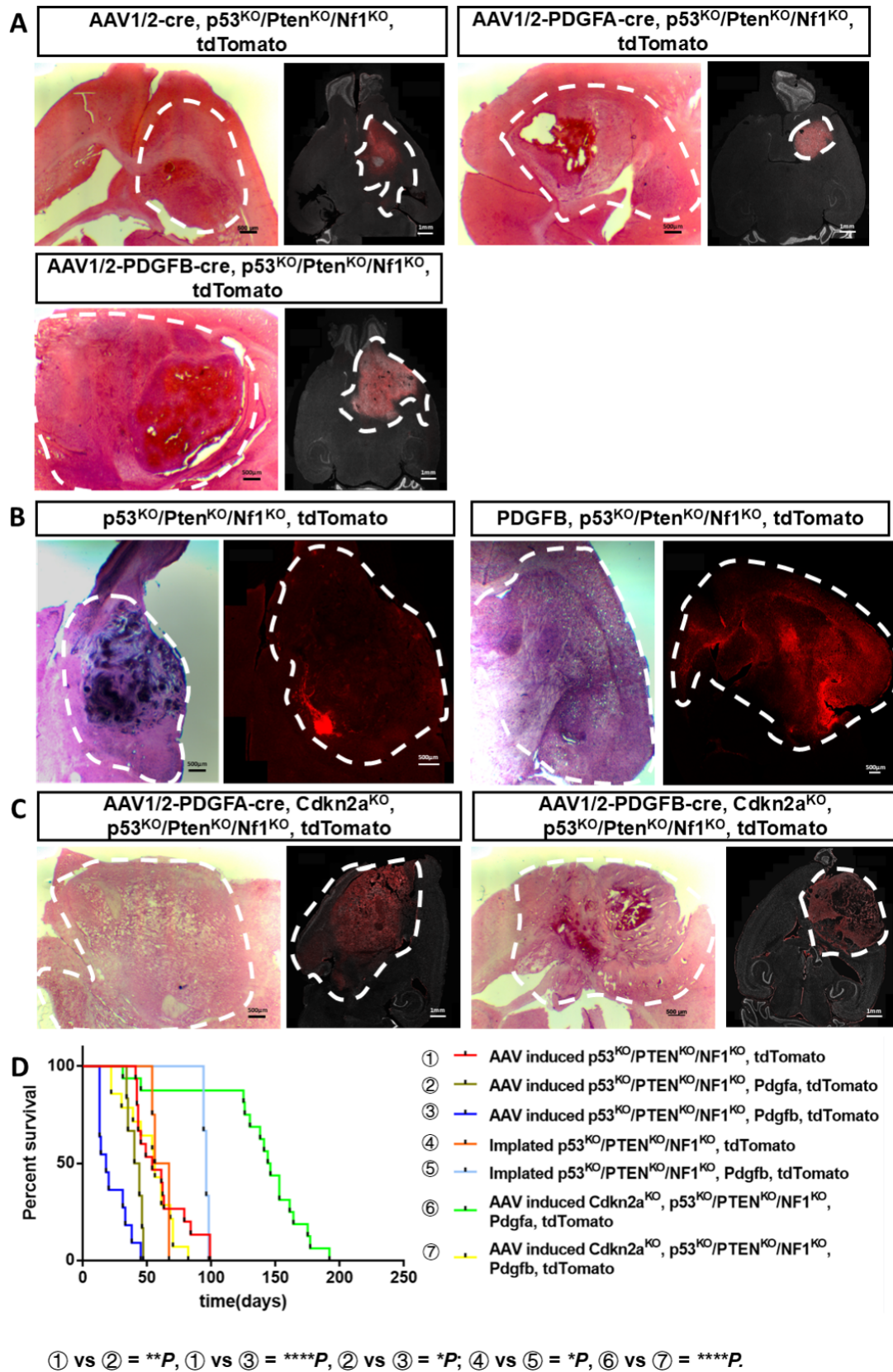


Figure 2 | Tumor take check and survival analysis of lineage-tracing mice GBM models recapitulating different human GBM subtypes

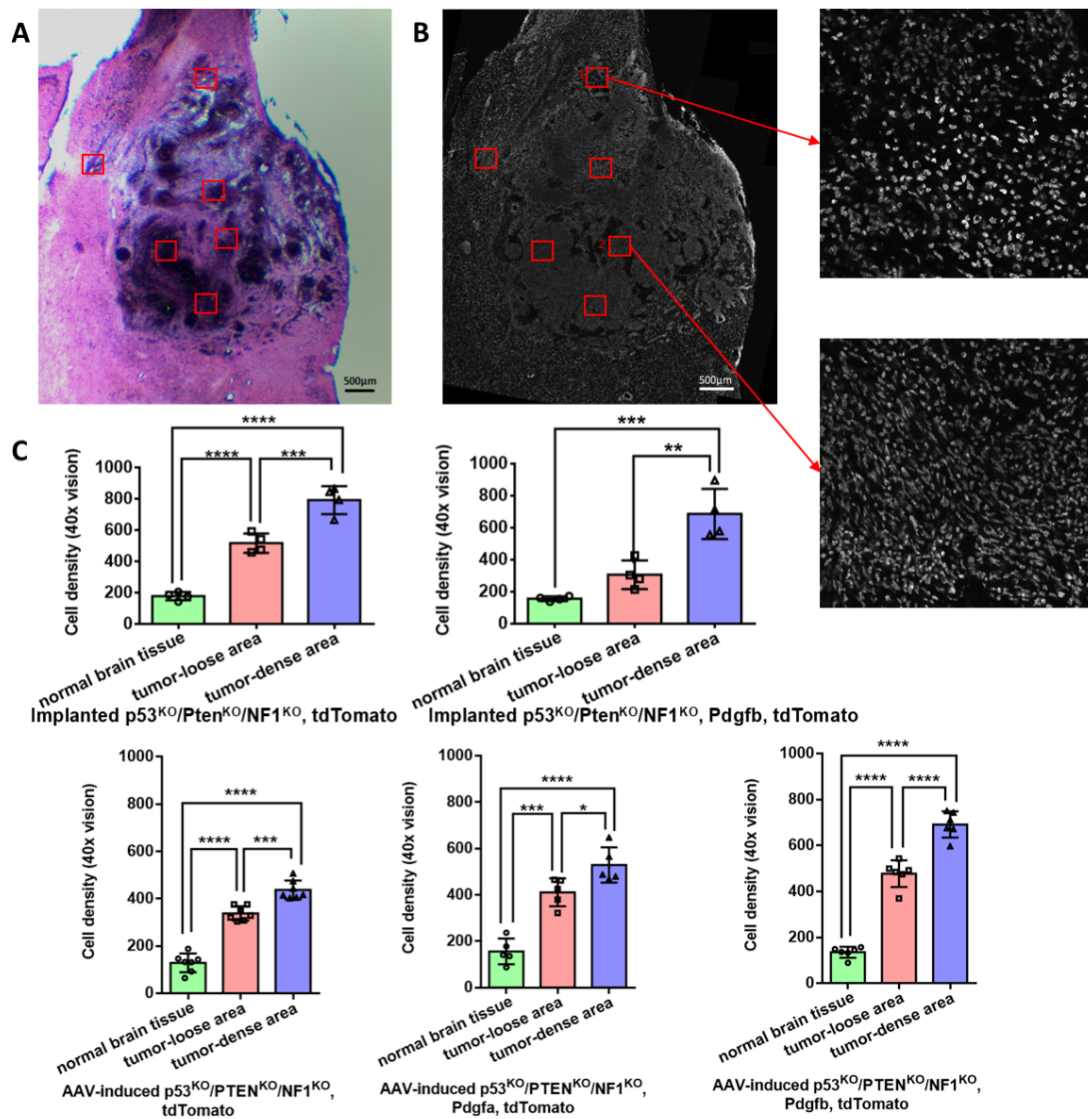
(A) Representative images of H&E staining and immunostaining of AAV induced

p53^{KO}/Pten^{KO}/Nf1^{KO}, tdTomato GBM models series. (B) Representative images of H&E staining and immunostaining of AAVs induced Cdkn2aKO, p53^{KO}/Pten^{KO}/Nf1^{KO}, tdTomato GBM models series. (C) Representative images of H&E staining and immunostaining of implanted transgenic GBM cells (p53^{KO}/Pten^{KO}/Nf1^{KO}, tdTomato or p53^{KO}/Pten^{KO}/Nf1^{KO}, Pdgfb, tdTomato) GBM models series. (D) Survival analysis of all GBM subtypes mice models. Statistical significance according to the log-rank (Mantel-Cox) test is expressed as * $P < 0.05$, ** $P < 0.01$, *** $P < 0.001$ and **** $P < 0.0001$. Scale bars and their length were shown on the pictures.

4.1.3 Definitions of different tumor regions and origins of pericytes

Glioblastoma was defined as a heterogeneous malignancy in the CNS [152]. In this experiment, I noticed that tumor cells were unevenly distributed in our GBM models. To investigate tumor heterogeneity, a method was established to divide the tumor into a tumor-core area and a tumor-invasive area based on the cell density in different tumor regions. Two consecutive brain slices were selected and H&E staining was performed to exclude the necrotic areas (Fig 3A) and immunostaining to count tumor cell numbers (Fig 3B), respectively. At least nine 40× magnification images in randomly selected non-necrotic visions were acquired from each slice. Three slices were obtained from each mouse, and three mice were selected from each GBM genotype. The cell density in each image was calculated using the ImageJ software with DAPI staining. Tumor areas with high cell density could be defined as tumor-core, whereas tumor fields with lower cell density belonged to the invasive tumor-rim. Thereby statistically reproducible, quantification data were defined to define tumor-invasive area or tumor-

core area for each transgenic tumor model. A *t*-test was used to examine the statistically significant difference of cell density for each tumor area (Fig 3C). As previous studies have demonstrated that pericytes in GBM can originate from both GSCs and the microenvironment, the origins of pericytes were defined by the co-localisation of tumor cells carrying the tdTomato reporter and PDGFRB immunostaining. Simultaneously, endogenous pericytes were defined as PDGFRB-positive but tdTomato-negative (Fig 3D).



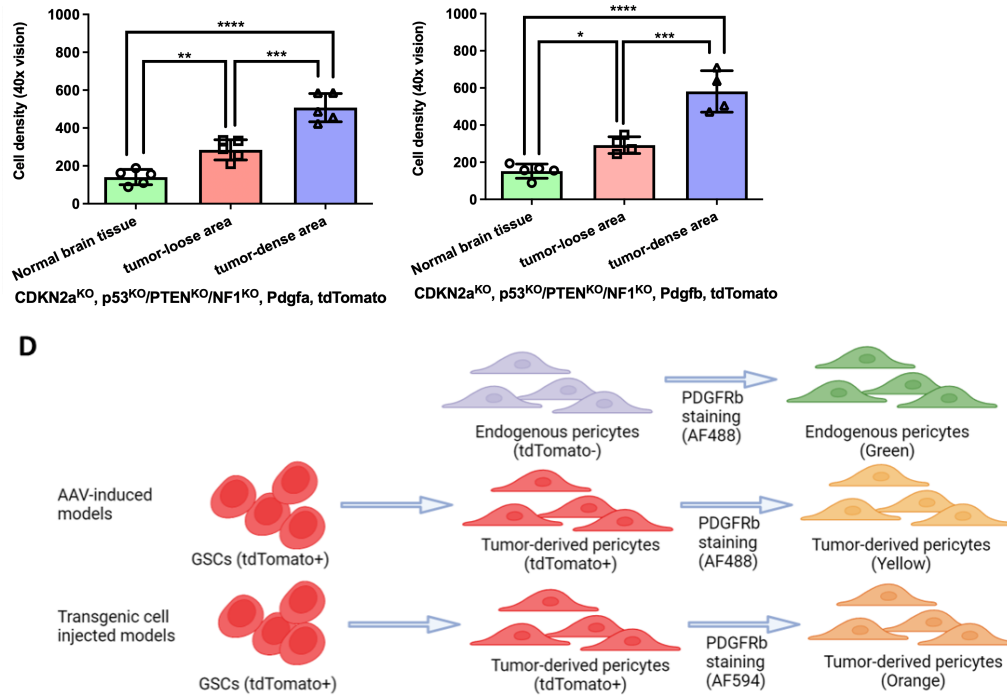


Figure 3 | Definitions of different tumor regions and origins of pericytes

(A) Representative H&E staining to present the induced tumor and necrotic areas (area with light colour within the tumor). (B) Representative immunostaining (DAPI) images showed how imaging sites were randomly selected. Magnified DAPI staining images were used to count cell density. (C) Cell density counting results showed cell number varies in different tumor areas (tumor-core and tumor-invasive area) in all GBM mice models. (D) Schematic diagram displayed the principle to define the origins of pericytes in GBMs.

4.1.4 Host and tumor equally generated pericytes in AAV-induced p53^{KO}/Pten^{KO}/Nf1^{KO} GBM models

In this experiment, tumor-derived pericyte coverage, endogenous pericyte coverage, and total pericyte coverage were calculated with ImageJ software using the following formulas:

- ◆ Total pericyte coverage = colocalised area of pericytes and vessels (PDGFRB+vessel marker)/vessel areas
- ◆ Tumor-derived pericyte coverage = colocalised area of tumor-derived pericytes and vessels (PDGFRB+tdTomato+vessel marker)/vessel areas.
- ◆ Endogenous pericyte coverage = total pericyte coverage – tumor-derived pericyte coverage.

Representative images of the AAV-induced p53^{KO}/Pten^{KO}/Nf1^{KO} GBM models are shown (Fig. 4A). The pericyte coverage results showed that PDGFB overexpression could upregulate the total pericyte coverage compared to non-overexpressing and PDGFA-overexpressing models in the tumor-core area, tumor-invasive area, and the entire tumor (Fig 4B). When pericytes were divided into tumor-derived and endogenous types, the results showed PDGFB overexpression upregulated pericyte coverage in both the tumor core and invasive area (Fig 4C and 4D). Furthermore, the results showed that in both tumor core area and tumor invasive area, the ratio of tumor-derived pericytes and endogenous pericytes showed non-significant differences, suggest tumor and host contributed roughly equal to the pericyte generation in AAV-induced p53^{KO}/Pten^{KO}/Nf1^{KO} GBM models (Fig 4C and 4D).

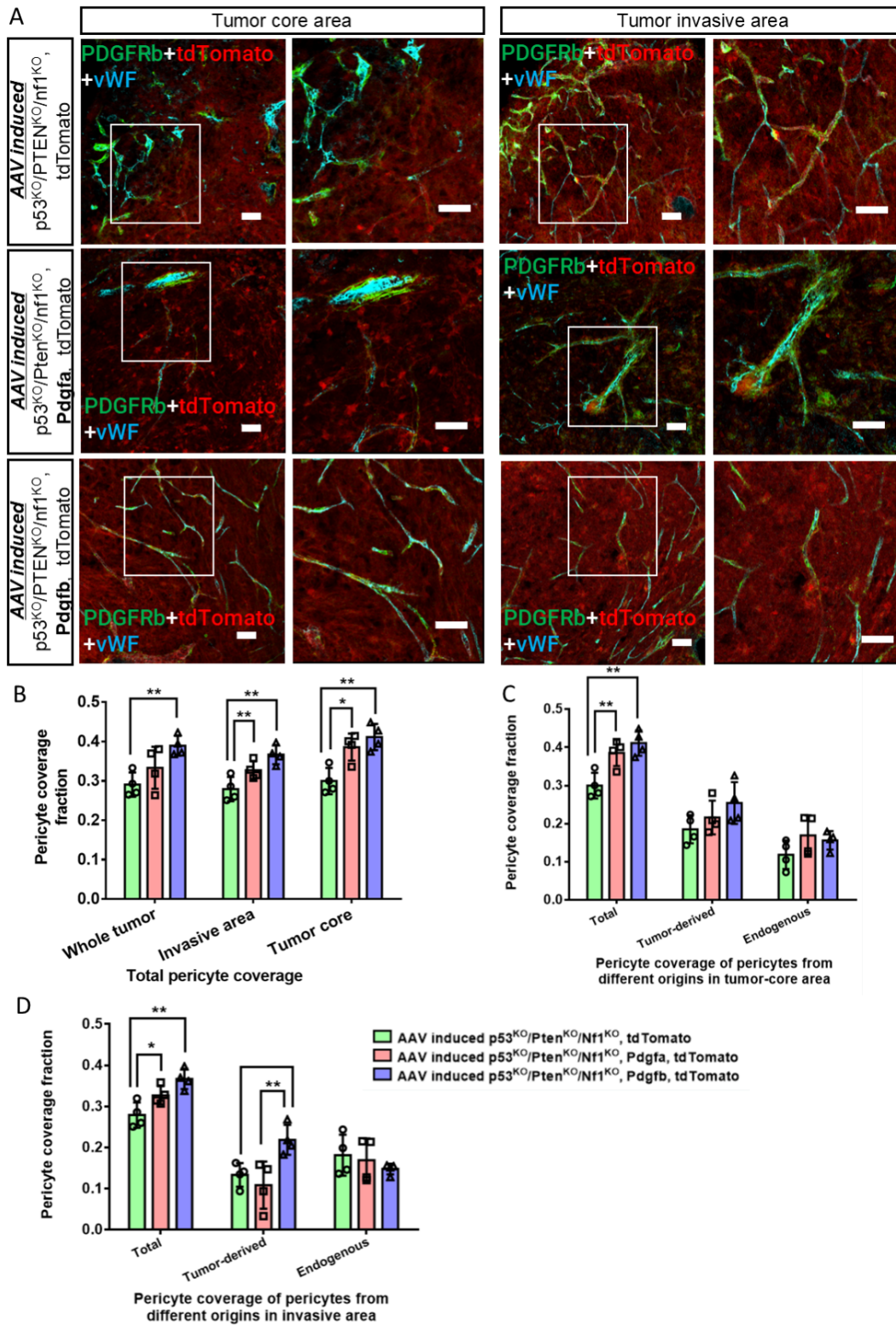


Figure 4 | PDGFB overexpression upregulated pericyte coverage in AAV-induced p53^{KO}/Pten^{KO}/Nf1^{KO} GBM models

(A) Representative images of AAV-induced GBM models present pericytes originating from different origins. (B) Pericyte coverage results in both tumor-core and tumor-

invasive areas when calculated without defining pericyte's origins. (C) Different originated pericyte coverage results in the tumor-core area. (D) Different originated pericyte coverage results in the tumor-invasive area. Statistical significance according to one-way ANOVA with post-hoc test is expressed as * $P < 0.05$, ** $P < 0.01$. Each dot shows the average data acquired from a single mouse. Values are presented as mean \pm SD. Scale bar = 50 μm .

4.1.5 The host and tumor equally generated pericytes in orthotopically injected transgenic p53^{KO}/Pten^{KO}/Nf1^{KO} GBM models

Representative images of the orthotopically implanted transgenic GBM models are shown (Fig. 5A). The pericyte coverage fraction was calculated. The results showed that PDGFB-overexpressing models had higher pericyte coverage than non-overexpressing models; however, the difference was not statistically significant (Fig 5B and 5C). Interestingly, the ratio of tumor-derived pericytes to endogenously derived pericytes was approximately 50:50 (Fig 5B and 5C).

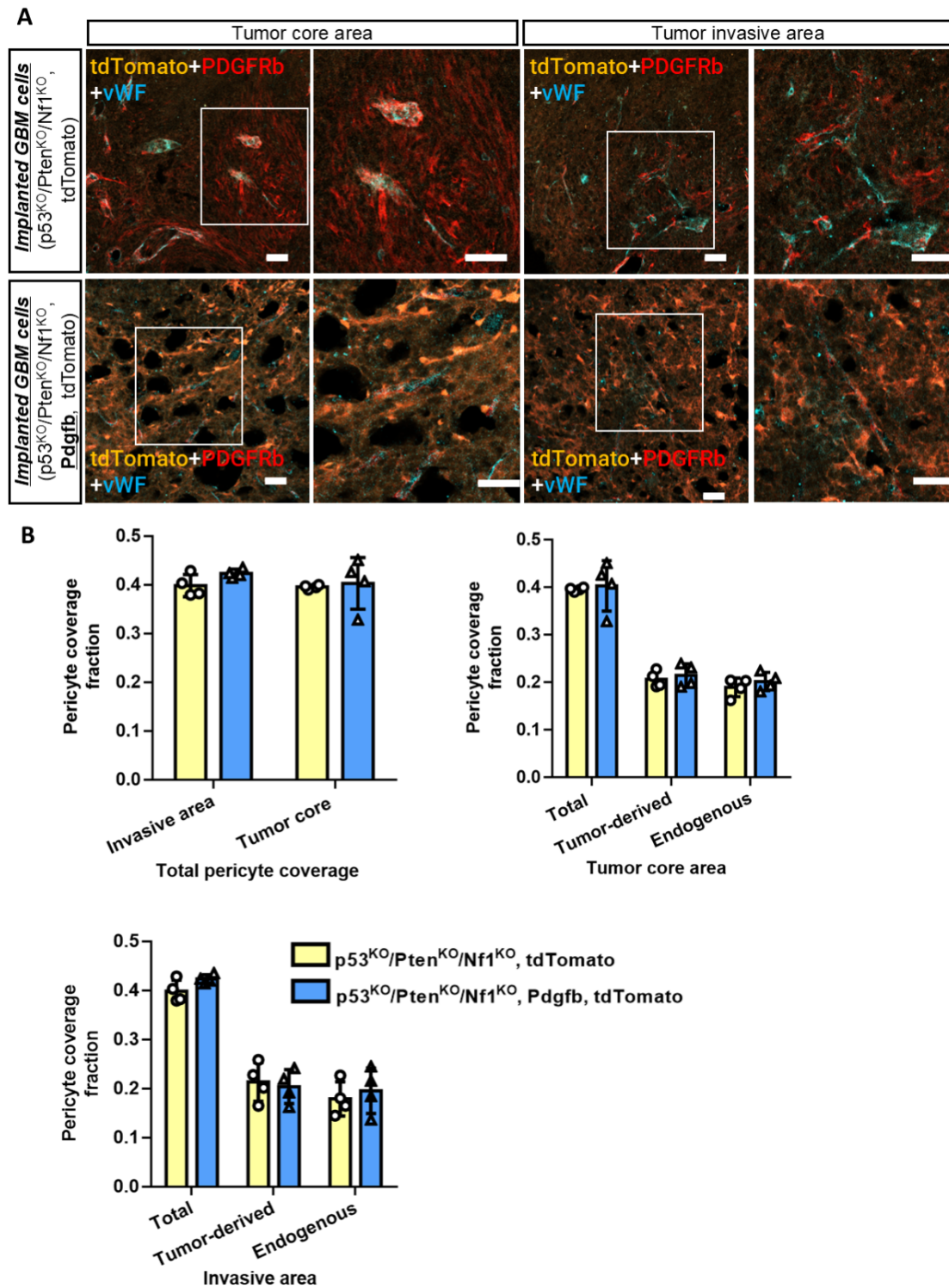


Figure 5 | Host and tumor equally generated pericytes in orthotopically injected transgenic p53^{KO}/Pten^{KO}/Nf1^{KO} GBM models

(A) Representative images of orthotopically implanted transgenic GBM models present pericytes originating from different origins. (B) Pericyte coverage results in both tumor-core and tumor-invasive areas when calculated without defining pericyte's origins. (C)

Different originated pericyte coverage results in the tumor-core area. (D) Different originated pericyte coverage results in the tumor-invasive area. Statistical significance according to one-way ANOVA with post-hoc test is expressed as ns = non-significant. Each dot shows the average data acquired from a single mouse. Values are presented as mean \pm SD. Scale bar = 50 μ m.

4.1.6 The host and tumor equally generated pericytes in CDKN2aKO and p53^{KO}/Pten^{KO}/Nf1^{KO} GBM models

Pericyte coverage of AAV-induced CDKN2aKO and p53^{KO}/Pten^{KO}/Nf1^{KO} models was calculated using the method described previously, and representative immunostaining images are shown (Fig. 6A). The results showed PDGFA-overexpression and PDGFB-overexpression models displayed similar pericyte coverage (Fig 6B and 6C), and pericytes originating from tumors accounted for approximately 50% of all pericytes, whereas the other 50% were host-generated pericytes (Fig 6B and 6C).

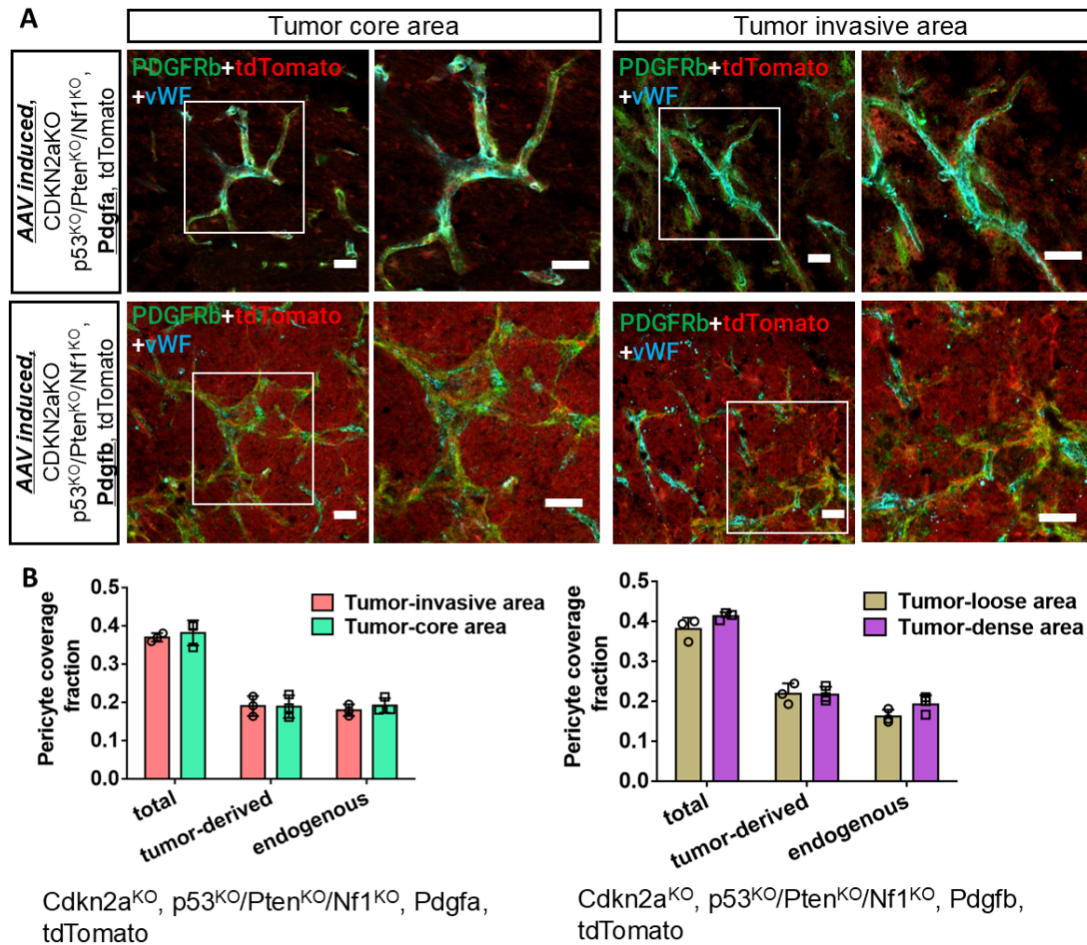


Figure 6 | Host and tumor equally generated pericytes in CDKN2aKO, p53^{KO}/Pten^{KO}/Nf1^{KO} GBM models

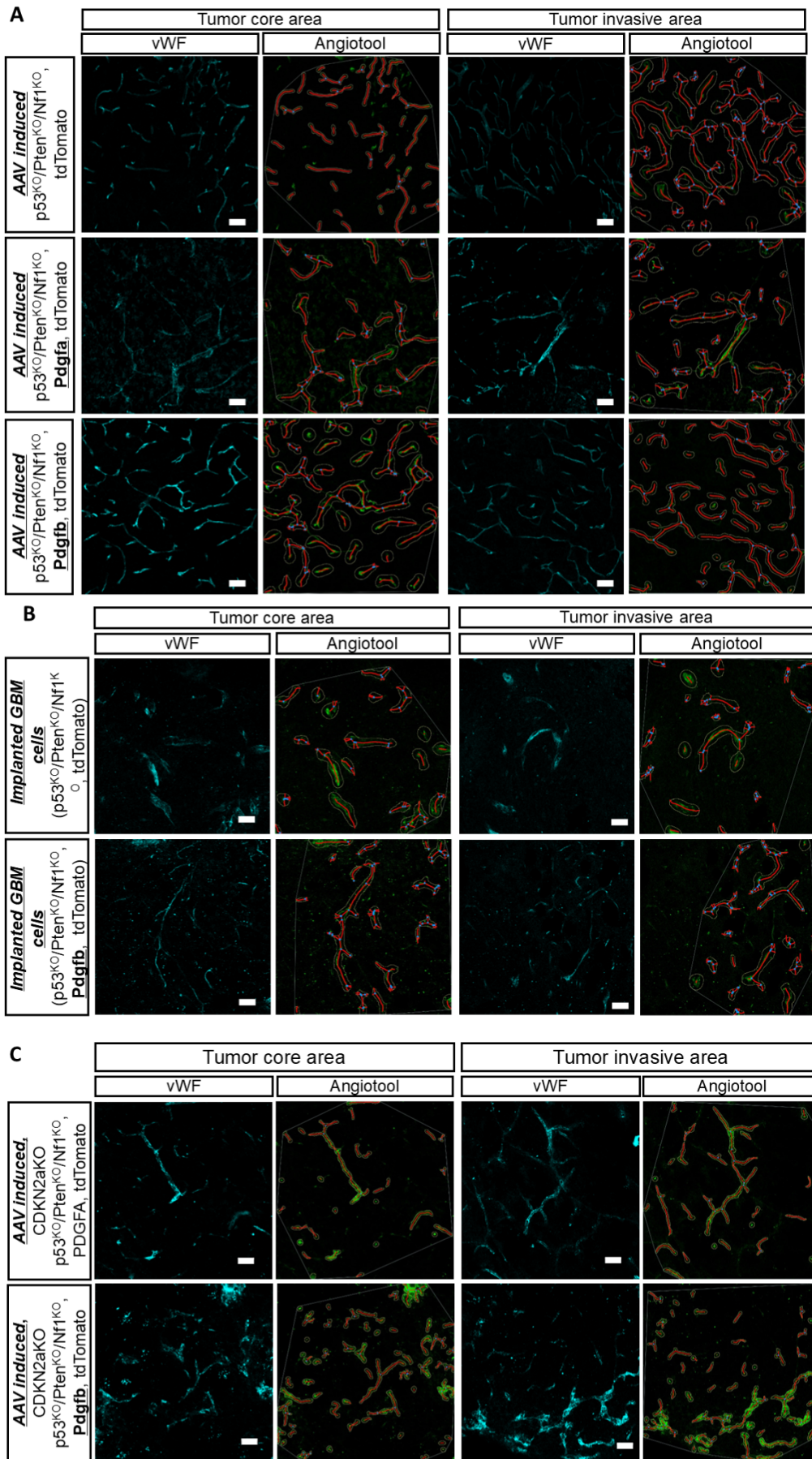
(A) Representative images of orthotopically implanted transgenic GBM models present pericytes originating from different origins. (B) Pericyte coverage results of pericytes from Different origins in both tumor-core and tumor-core areas of Cdkn2aKO, p53^{KO}/Pten^{KO}/Nf1^{KO} and tdTomato GBM models. (C) Pericyte coverage results of pericytes from Different origins in both tumor-core and tumor-core areas of Cdkn2aKO, p53^{KO}/Pten^{KO}/Nf1^{KO}, Pdgfb and tdTomato GBM models. Statistical significance according to one-way ANOVA with post-hoc test is expressed as ns = non-significant. Each dot shows the average data acquired from a single mouse. Values are presented as mean ± SD. Scale bar = 50 μm.

4.1.7 Vasculature analysis of all GBM subtypes.

AngioTool software was used to analyse the tumor vasculature of AAV-induced p53/PTEN/NF1 knockout models (Fig 7A), transgenic cell line-injected models (Fig 7B), and AAV-induced CDKN2aKO, p53^{KO}/Pten^{KO}/Nf1^{KO} models (Fig 7C). The vessel area is the area occupied by vessel segments in the image. The vessel junction number refers to the number of vessel segment connection points in an image. The total vessel length is the sum of the Euclidean distances between the pixels of all the vessels in the image. The Average vessel length represents the mean length of all vessels in the image.

In tumor-core area of vessel area parameter, AAV-induced PDGFA and PDGFB overexpressing p53^{KO}/Pten^{KO}/Nf1^{KO} (abbreviated as AAV-PDGFA p53/Pten/Nf1 KO and AAV-PDGFB p53/Pten/Nf1 KO) models showed higher vessel area than orthotopically implanted p53^{KO}/Pten^{KO}/Nf1^{KO} model, and AAV-PDGFB p53/Pten/Nf1 KO model showed higher vessel area than AAV induced Cdkn2a^{KO}, p53^{KO}/Pten^{KO}/Nf1^{KO}, Pdgfa (abbreviated as AAV-PDGFA Cdkn2aKO) model. In tumor invasive area, vessel area of AAV- PDGFB p53^{KO}/Pten^{KO}/Nf1^{KO} model was higher than the vessel area of both orthotopically implanted p53/Pten/Nf1 KO model and AAV-PDGFA Cdkn2aKO model (Fig 7D). Moreover, in junction numbers parameter, in the tumor core area, AAV induced p53^{KO}/Pten^{KO}/Nf1^{KO} model had higher numbers than AAV-PDGFB p53/Pten/Nf1 KO, orthotopically implanted p53^{KO}/Pten^{KO}/Nf1^{KO}, Pdgfb, AAV-PDGFA Cdkn2aKO and AAV-PDGFB Cdkn2aKO models. In tumor invasive area, AAV-PDGFA p53/Pten/Nf1 KO model had higher numbers than AAV-PDGFB p53/Pten/Nf1 KO model and AAV-PDGFA Cdkn2aKO model (Fig 7D). In total vessel

length result of tumor core area, AAV induced p53^{KO}/Pten^{KO}/Nf1^{KO} model showed higher parameters than orthotopically implanted PDGFB, p53/Pten/Nf KO, AAV-PDGFA Cdkn2aKO and AAV-PDGFB Cdkn2aKO models; AAV-PDGFA p53/Pten/Nf1 KO model showed higher parameters than in AAV-PDGFB p53/Pten/Nf1 KO model, orthotopically implanted p53^{KO}/Pten^{KO}/Nf1^{KO} model, AAV-PDGFA Cdkn2aKO and AAV-PDGFB Cdkn2aKO models; AAV-PDGFB p53/Pten/Nf1 KO model showed higher parameters than orthotopically injected p53^{KO}/Pten^{KO}/Nf1^{KO} model. Meanwhile in tumor invasive area, AAV-cre p53/Pten/Nf1 KO model showed higher parameters than in AAV-PDGFA Cdkn2aKO model; AAV-PDGFA p53/Pten/Nf1 KO model showed higher parameters than in orthotopically implanted p53^{KO}/Pten^{KO}/Nf1^{KO} model and AAV-PDGFA Cdkn2aKO model (Fig 7D). At last, in average vessel length area parameter, only in tumor core significant differences were observed between AAV induced p53/Pten/Nf1 KO model with orthotopically implanted p53^{KO}/Pten^{KO}/Nf1^{KO} and PDGFB overexpressing models, also AAV-PDGFA Cdkn2aKO and AAV-PDGFB Cdkn2aKO models (Fig 7D). These results demonstrated that vessel patterns vary a lot among different GBM models.



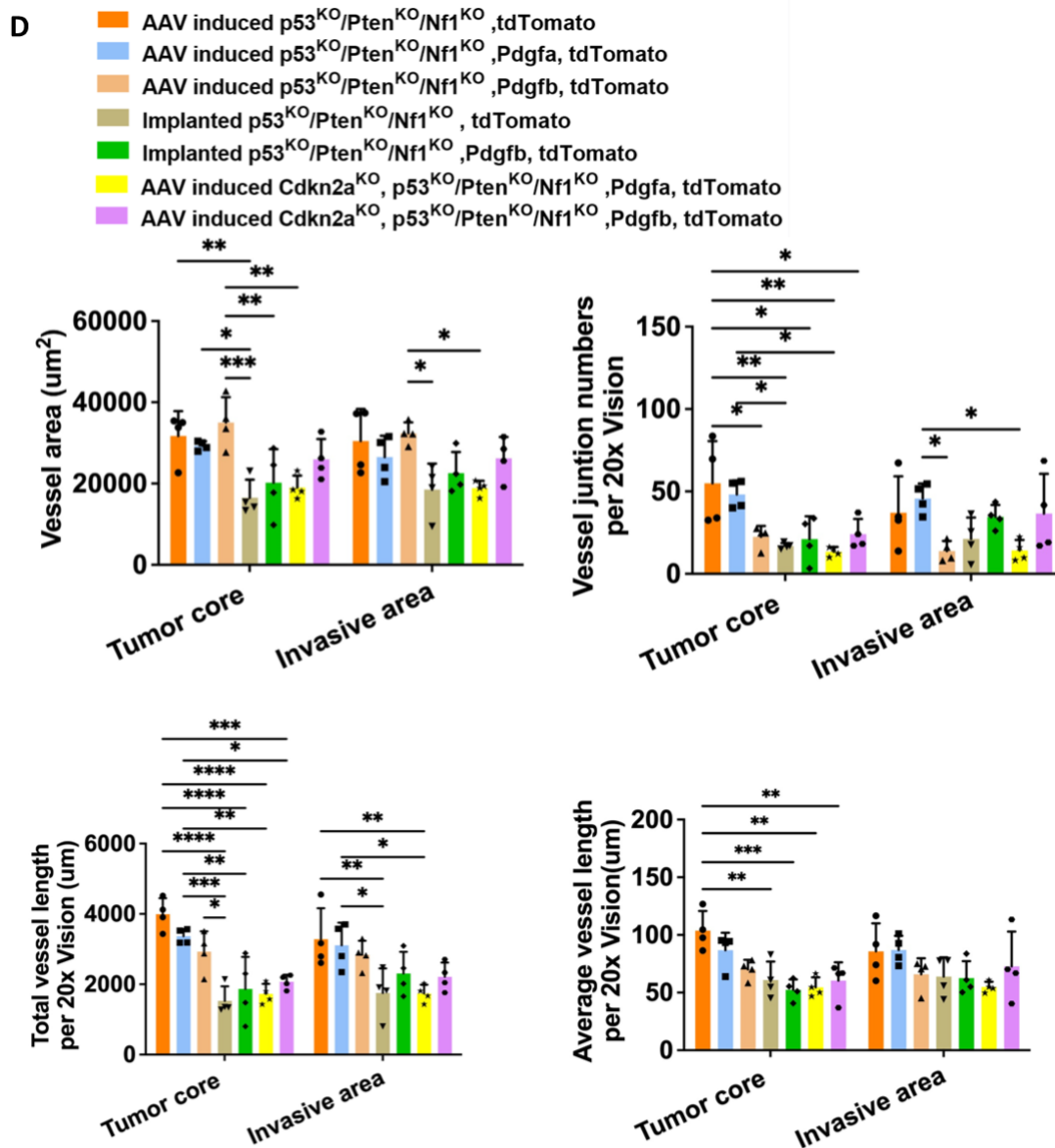


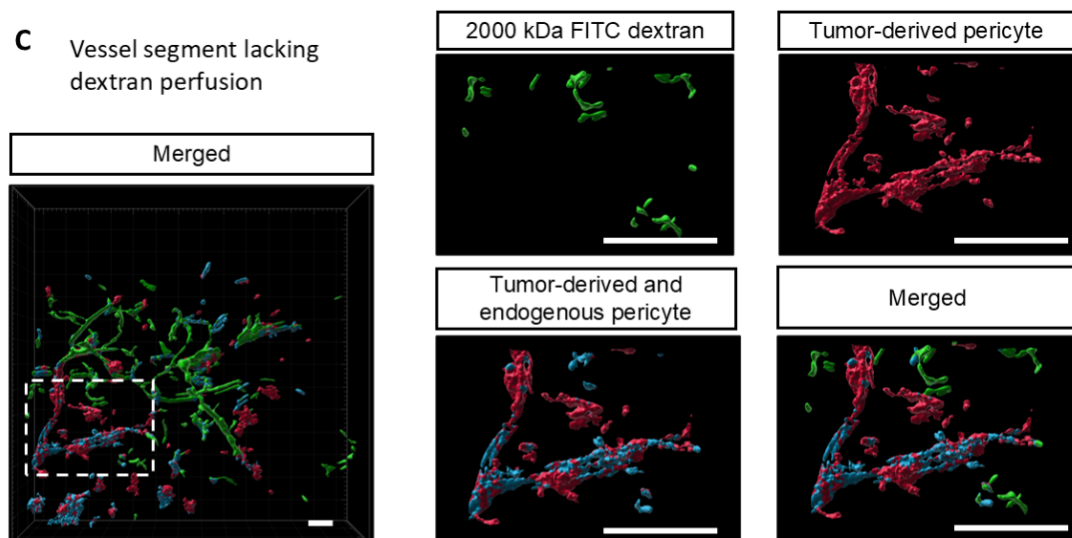
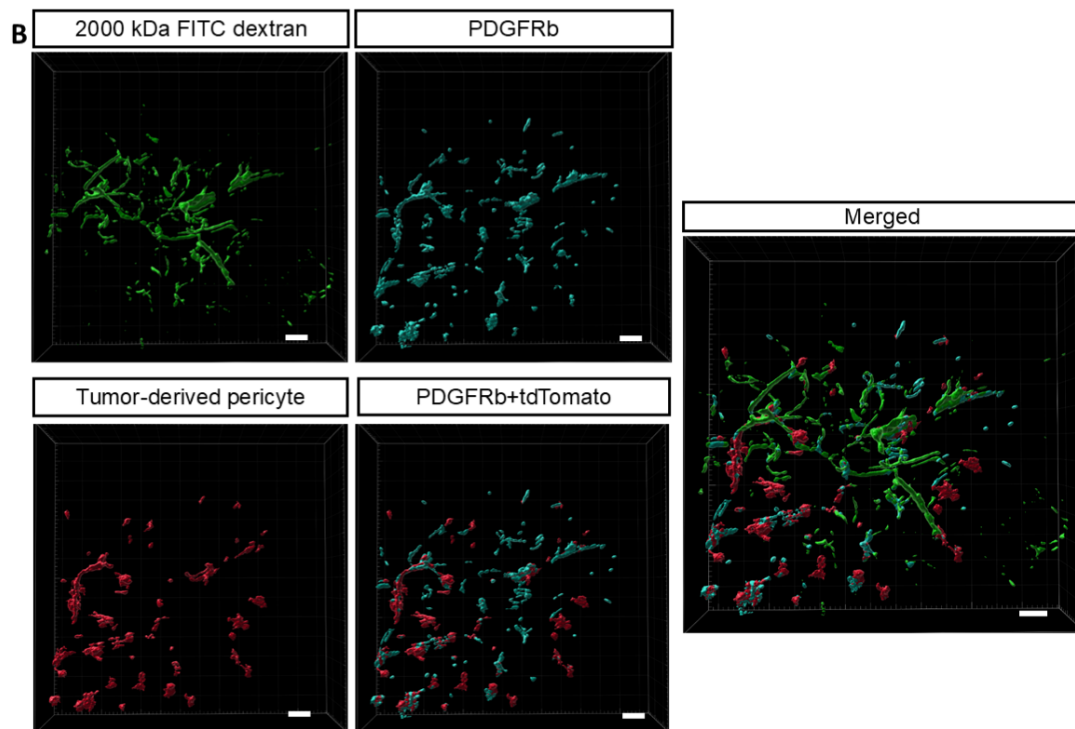
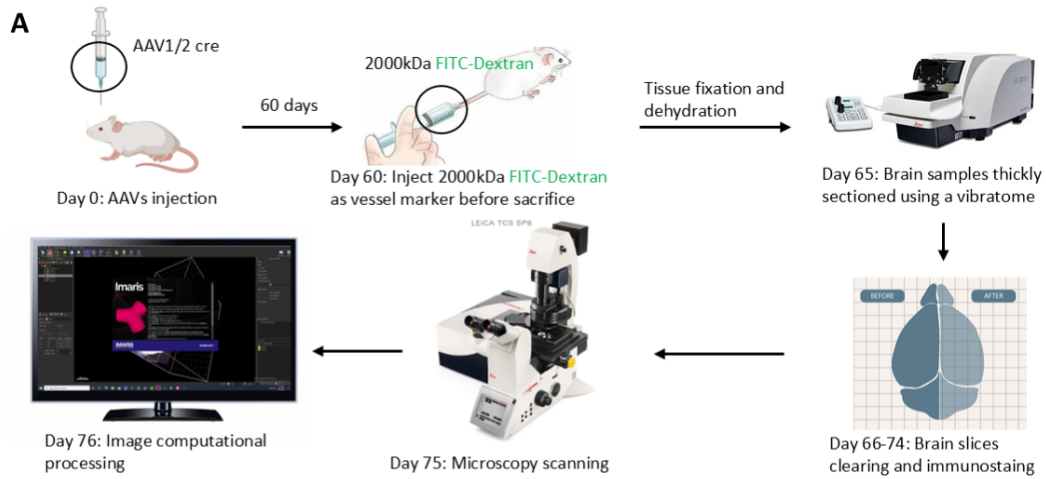
Figure 7 | Vasculature analysis of all GBM subtypes

(A) Representative images of CD31 staining and AngioTool analysed images of AAV-induced p53^{ko}/Pten^{KO}/Nf1^{KO}, tdTomato; p53^{ko}/Pten^{KO}/Nf1^{KO}, Pdgfa, tdTomato and p53^{ko}/Pten^{KO}/Nf1^{KO}, Pdgfb, tdTomato models. (B) Representative images of CD31 staining and AngioTool analysed images of orthotopically implanted transgenic GBM (p53^{ko}/Pten^{KO}/Nf1^{KO}, tdTomato and p53^{ko}/Pten^{KO}/Nf1^{KO}, Pdgfb, tdTomato) models. (C) Representative images of von Willebrand Factor (vWF) staining and AngioTool analysed images of AAV-induced Cdkn2a^{KO}, p53^{ko}/Pten^{KO}/Nf1^{KO}, Pdgfa, tdTomato and Cdkn2a^{KO}, p53^{ko}/Pten^{KO}/Nf1^{KO}, Pdgfb, tdTomato models. (D) Vasculature analysis parameters results of all GBM subtypes. Statistical significance according to one-way

ANOVA with post-hoc test is expressed as * $P < 0.05$, ** $P < 0.01$, *** $P < 0.001$ and **** $P < 0.0001$. Each dot shows the average data acquired from a single mouse. Values are presented as mean \pm SD. Scale bar = 50 μm .

4.1.8 Tissue clearing of mice GBM samples and 3D-reconstruction of tumor vessel structure

To visualise tumor vessel structures, IMARIS software was used to complete the 3D-reconstruction of tumor vessels (Fig 8A). 2000kDa FITC-dextran was injected into the mice before sacrifice to label the vessel lumen and tdTomato-labelled tumor cells. PDGFRB staining was performed to label pericytes. Here the vessel lumens are displayed in green, tumor-derived pericytes are shown in a PDGFRB⁺ and tdTomato⁺ colocalised panel in red, endogenous pericytes in a PDGFRB⁺ but tdTomato⁻ panel in cyan, and a merged image (Fig 8B-D). In the 3D reconstructed images, tumor-derived pericytes and endogenous pericytes were clearly showed covering tumor vessels (Fig 8B). Interestingly, there are some pericytes, mainly tumor-derived, were found sitting in the area lacking dextran perfusion (Fig 8B-D). That may suggest tumor-derived pericytes may contributed more in low-perfusion areas in GBM.



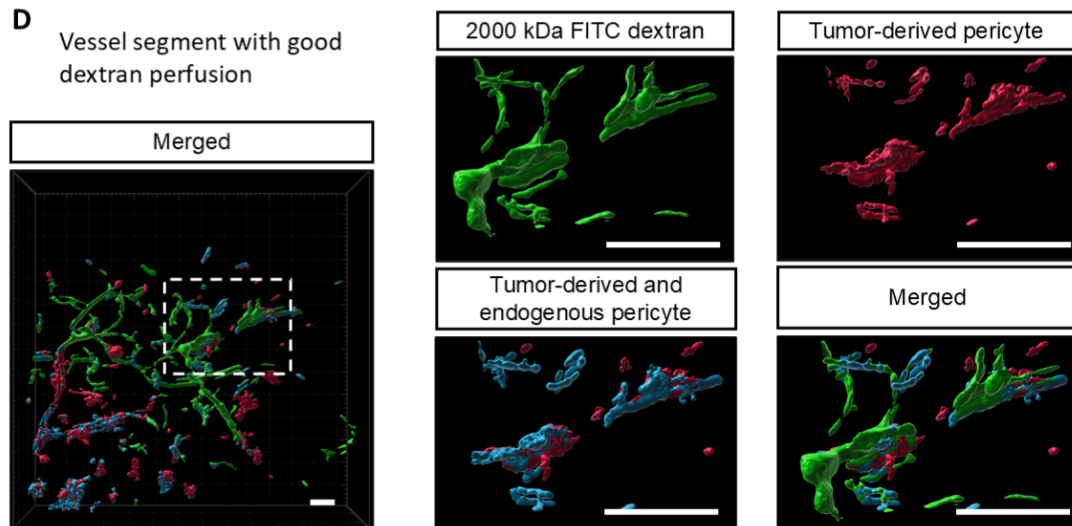


Figure 8 | Tissue clearing of mice GBM samples and 3D-reconstruction of tumor vessel structure

(A) Flow chart of GBM samples tissue clearing, immunostaining, and 3D reconstruction process. AAVs were injected to mice brains at day0. 2000kDa FITC-dextran were injected through mice tail vein after 60 days tumor growth, followed by tissue fixation. Brain samples were cut into 200 μ m sections using a vibratome. After the tissue clearing and immunostaining procedure was finished, samples were scanned by confocal microscopy, and the 3D reconstruction was performed with IMARIS software. (B) The 3D-reconstructed images present tumor vessel structure of advanced AAV-induced p53^{ko}/Pten^{KO}/Nf1^{KO}, tdTomato (sacrificed at 60 d.p.o). (C) Magnified 3D-reconstructed images present a vessel segment lacking dextran perfusion. (D) Magnified 3D-reconstructed images present a vessel segment with good dextran perfusion. Scale bar = 50 μ m.

4.2 Pericytes ablation could upregulate BTB permeability in recurrent GBM mice models

4.2.1 The induction of pericyte depleted relapse GBM mice models

To induce relapse in GBM models, GL261-WT, a mouse tumor cell line, was transfected with a lentivirus containing GFP-tagged herpes simplex virus thymidine kinase (HSVTK-GFP) to generate a new tumor cell line (GL261-HSVTK) that could be killed after ganciclovir (GCV) treatment (Fig 9A) [178]. After inoculation of GL261-HSVTK cells in mice and growth for approximately 18 days, GCV was administered to mice by a one-time intraperitoneal injection (i.p.), and the mice were sacrificed when symptomatic. Tumor samples collected at different time points showed the successful induction of GBMs (Fig 9B). In this study, a pericyte lineage depletion model conditionally expressing diphtheria toxin-A (PDGFRB::creERT2, Rosa26-tdTomato, Rosa26-iDTA, abbreviated as PDGFRB-iDTA) was used to evaluate the functions of endogenous pericytes in different stages of recurrent GBM mice models. Three groups were included in this experiment including a control group (PDGFRB::creERT2, Rosa26-tdTomato, abbreviated as PDGFRB-reporter), and two pericyte depletion groups (early depleted group and late depleted group). In the early depletion group, tamoxifen was administered on days 33–35 after tumor cell inoculation (16–18 days after GCV administration) to ablate pericytes in the early stage of tumor relapse (Fig 9C). In the late-depletion group, tamoxifen was administered 44–46 days after tumor inoculations (27–29 days after GCV application) to ablate the pericytes during the late recurrent stage (Fig 9C). 70kDa biotin-dextran was injected through the tail veins of all mice before sacrifice (Fig 9C).

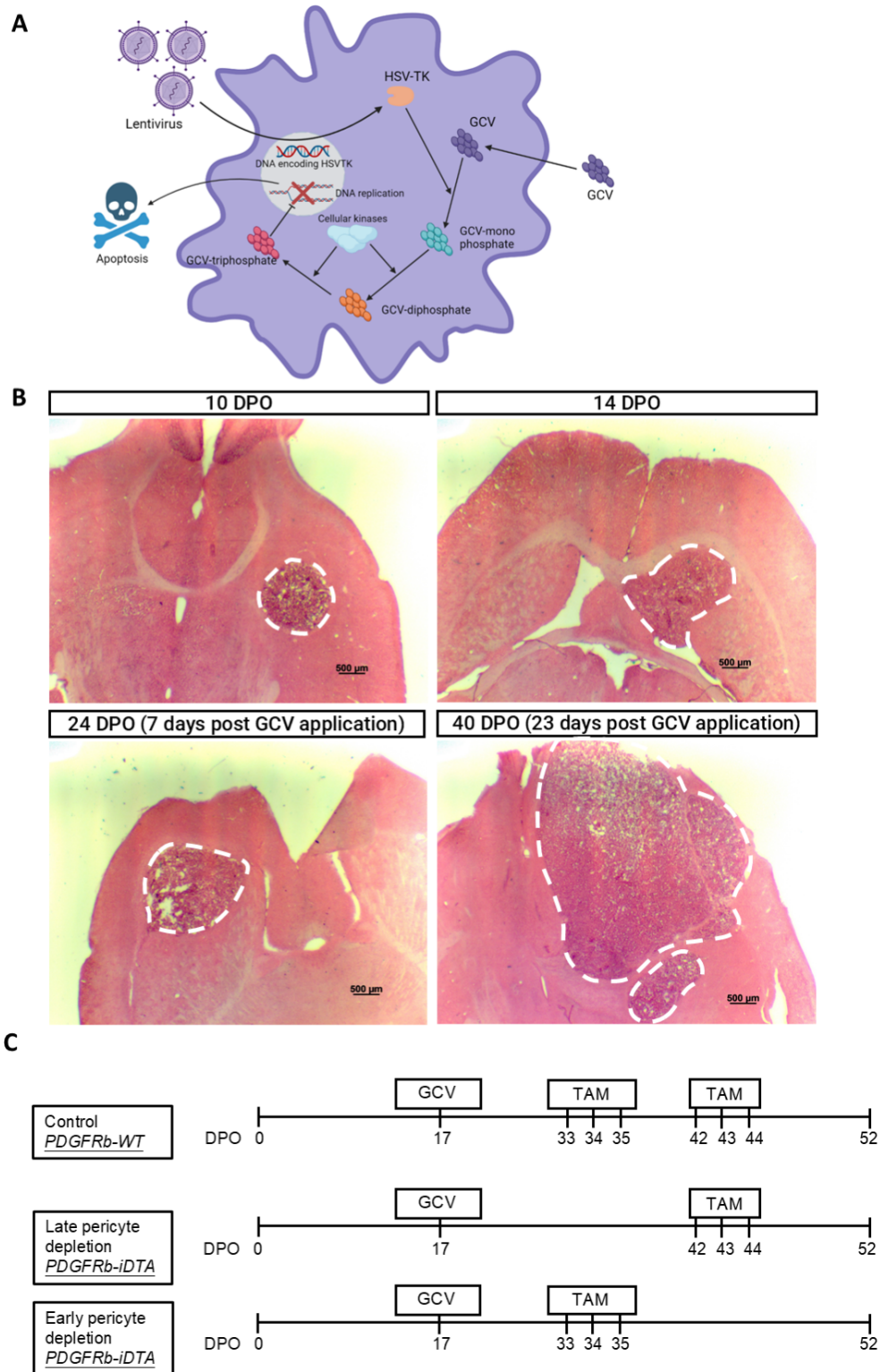


Figure 9 | Pericyte conditionally depleted relapse GBM models induction

(A) Schematic diagram presents cell-death induction in the GL261-HSVTK cell line. (B) Representative H&E-stained primary or recurrent GBM tumor images on different time-points after tumor implantation and ganciclovir (GCV) application. (C)

Experimental Schematic diagram of the experimental procedure in control (PDGFRB-WT), late pericyte depletion group (PDGFRB-iDTA), and late pericyte depletion group (PDGFRB-iDTA). TAM indicates tamoxifen injection days. Brains were harvested in all groups at day 52 or when mice were symptomatic.

4.2.2 Early stage pericytes ablation significantly opened BTB.

Under physiological conditions, 70kDa dextran cannot cross the BBB and enter the CNS. However, under pathological conditions, such as GBM, 70kDa dextran can escape from the vessel lumen and reach the tumor parenchyma. This allows measuring the permeability of the BTB by analysing the dextran distribution inside the tumors. Mice from all three groups (control and two ablated groups) were imaged using confocal microscopy and analysed using the ImageJ software (Fig 10A). The density of dextran entering the tumor parenchyma (leaked dextran) in control and late-depleted mice was similar (Fig 10B). However, in early depleted mice, the density of leaked dextran was significantly higher (Fig 10B). These results revealed that early ablation of pericytes significantly increased vascular permeability; however, late-stage pericyte depletion showed no obvious effect on vascular permeability when compared with controls.

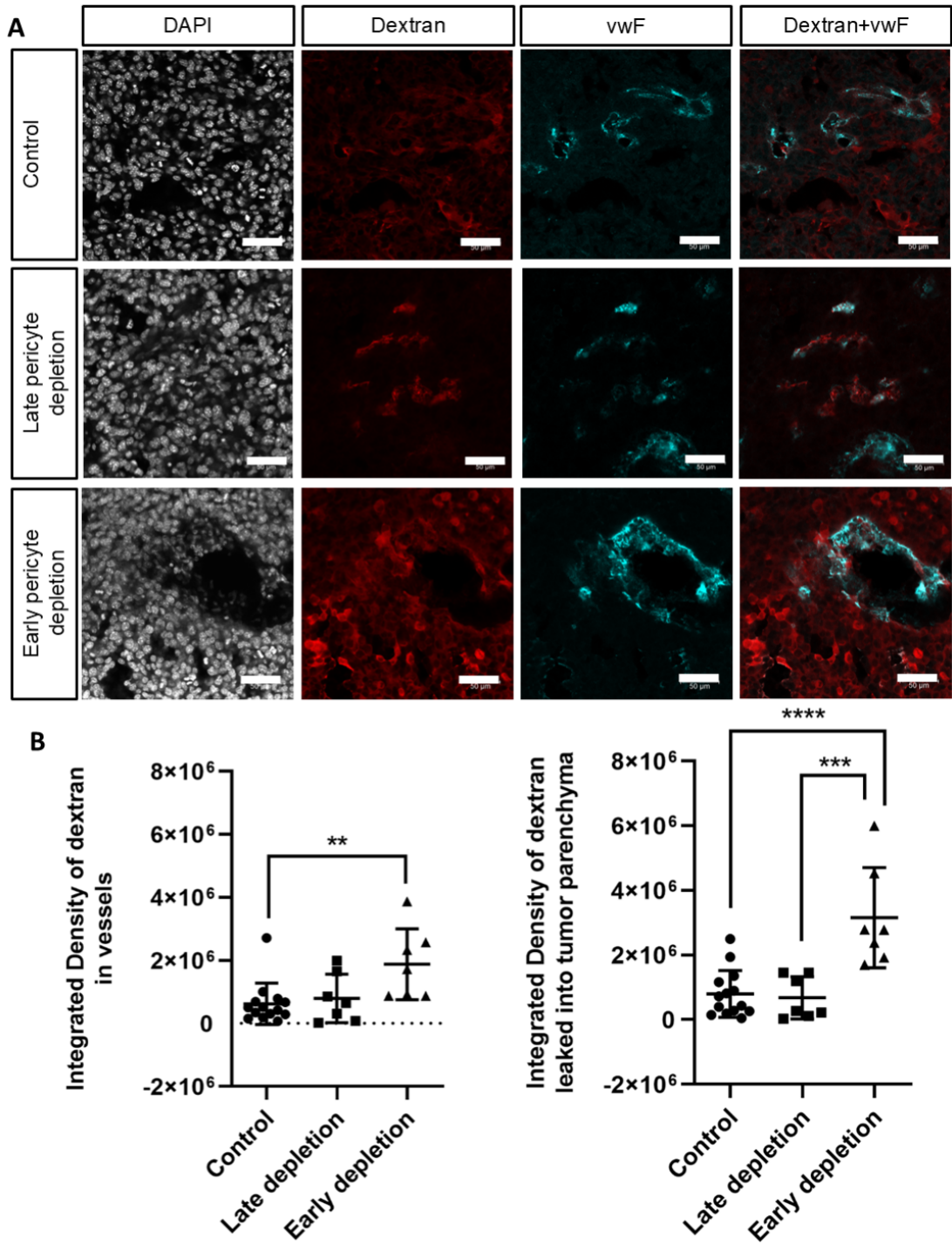


Figure 10 | Early stage pericytes ablation significantly opened BTB

(A) Representative images of 70kDa biotin-dextran and vWF staining of control, late pericyte depletion and early pericyte depletion groups. (B) Dextran leakiness results of all groups. Statistical significance according to one-way ANOVA with post-hoc test is expressed as ** $P < 0.01$, *** $P < 0.001$ and **** $P < 0.0001$. Each dot shows the average data acquired from a single mouse. Values are presented as mean \pm SD. Scale

bar = 50 μm .

4.2.3 Vasculature analysis of relapse GBM models

Pericytes play a vital role in tumor angiogenesis. To investigate whether pericyte ablation potentially affects tumor angiogenesis in relapsed GBM, previously described AngioTool software was used to analyse the tumor vasculature (Fig 11A). The results showed that the vessel patterns were not significantly different among the three groups (Fig 11B-E).

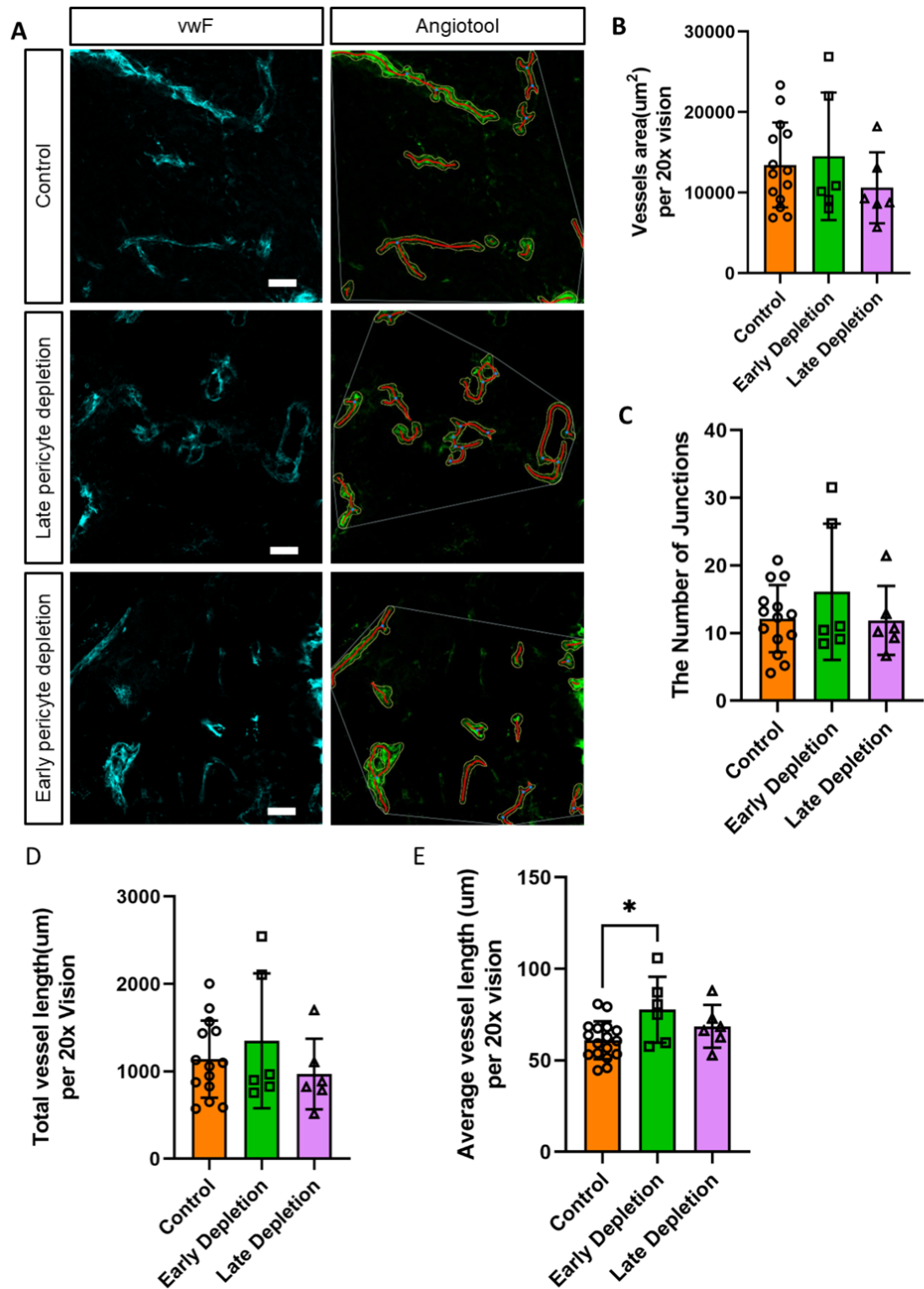


Figure 11 | Vasculature analysis of relapse GBM models

(A) Representative vWF staining images and AngioTool analysed images of all three groups relapse GBM models. (B) Results of vessel area parameters in AngioTool vasculature analysis. (C) Junction numbers parameters in AngioTool vasculature

analysis. (D) Results of total vessel length in AngioTool vasculature analysis. (E) Results of average vessel length parameters in AngioTool vasculature analysis. Statistical significance according to one-way ANOVA with post-hoc test is expressed as * $P < 0.05$. Each dot shows the average data acquired from a single mouse. Values are presented as mean \pm SD. Scale bar = 50 μm .

4.3 Full-time BAPN application increased BTB permeability in primary GBMs

4.3.1 Full-time BAPN treatment could suppress tumorigenesis

To evaluate the potential effects of BAPN in primary GBMs, BAPN was applied (dissolved in drinking water) to mice orthotopically implanted with GBM cells at three different time frames: full-time treatment (4–18 days post operation, d.p.o), early-stage treatment (4–10 d.p.o), and late-stage treatment (11–17 d.p.o) (Fig 12A). Tumor volume was calculated with H&E staining to measure tumor uptake (Fig 12B). The results showed that the full-time BAPN treatment of primary GBMs suppressed tumorigenesis (Fig 12C). However, part-time treatment had no obvious effects on tumor growth (Fig 12C).

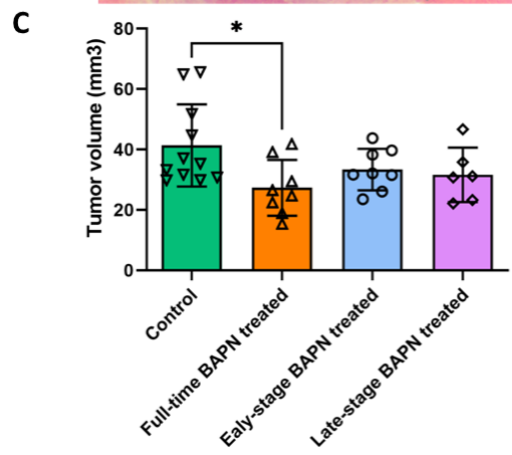
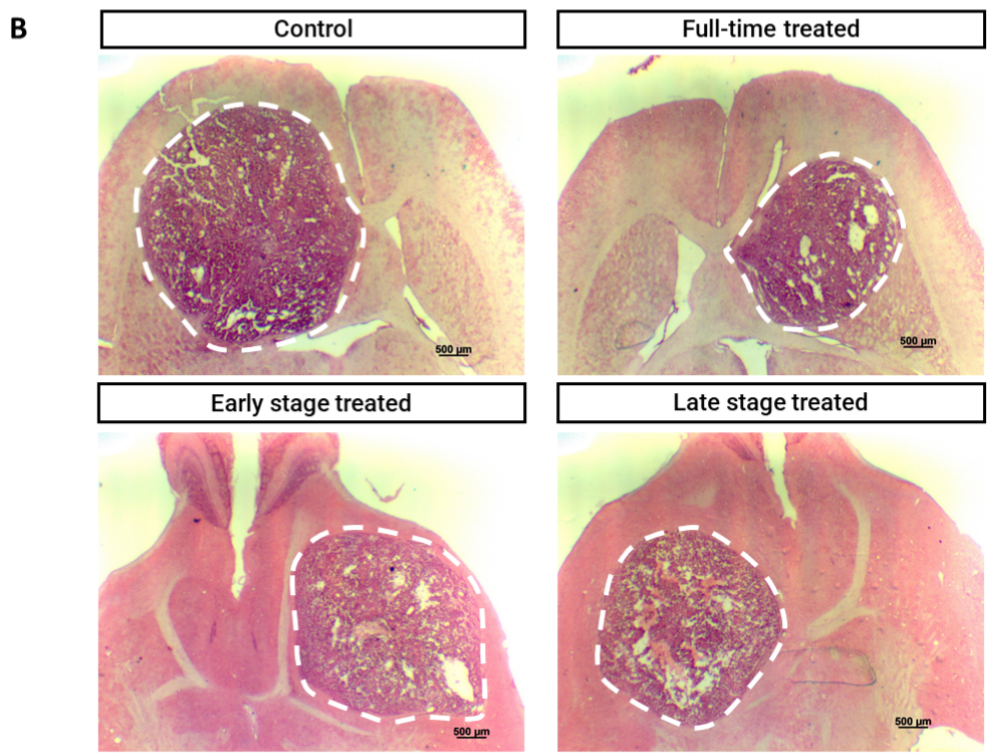
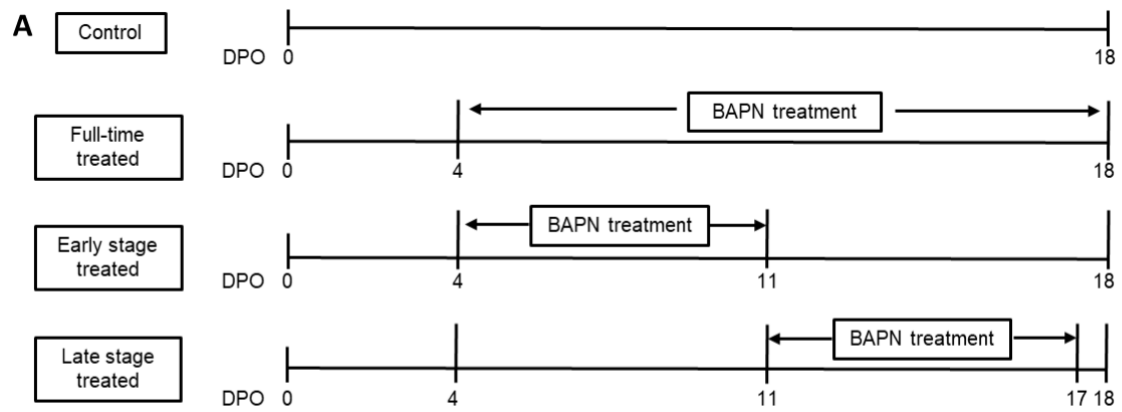


Figure 12 | Full-time BAPN treatment could suppress tumorigenesis

(A) Schematic diagram of the experimental procedure in control (no treatment), full-

time BAPN treatment, early-stage BAPN treatment and late-stage BAPN treatment on GL261wt cells implanted wild-type mice. All mice brain samples were harvested at day 18 post-tumor implantation. (B) Representative H&E staining images of GBMs of different groups. (C) Tumor volume calculation results of control and all BAPN-treated groups. Statistical significance according to one-way ANOVA with post-hoc test is expressed as * $P < 0.05$. Each dot shows the average data acquired from a single mouse. Values are presented as mean \pm SD. Scale bar = 500 μm .

4.3.2 Full-time BAPN treatment up-regulated Evans blue leakiness in tumor parenchyma

To determine whether BAPN treatment could interfere with BTB function in primary GBMs, Evans blue dye (EB), which has a molecular weight similar to 70kDa dextran, was injected through the tail vein before the mice were sacrificed to investigate EB extravasation in the tumor parenchyma (Fig 13A). The results showed that EB extravasation was significantly increased in full-time treated tumors compared to that in controls (Fig 13B). Considering the tumorigenic suppressive effects of BAPN, the EB extravasation results were normalised to the average tumor volume. The normalised results showed that full-time treatment significantly improved BTB permeability (Fig 13C). However, interestingly, in early- or late-stage treated mice, EB extravasation showed no obvious differences from controls (Fig 13C). This experiment confirmed that full-time BAPN treatment affects open GBM BTBs; however, part-time treatments had no significant efficacy.

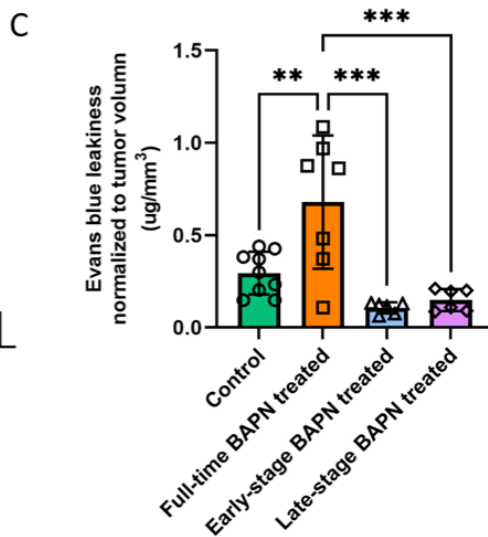
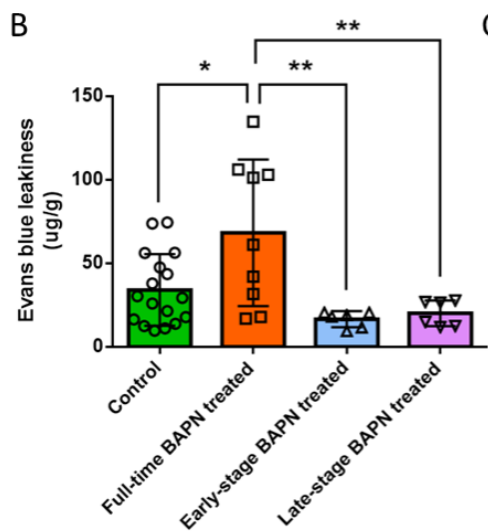
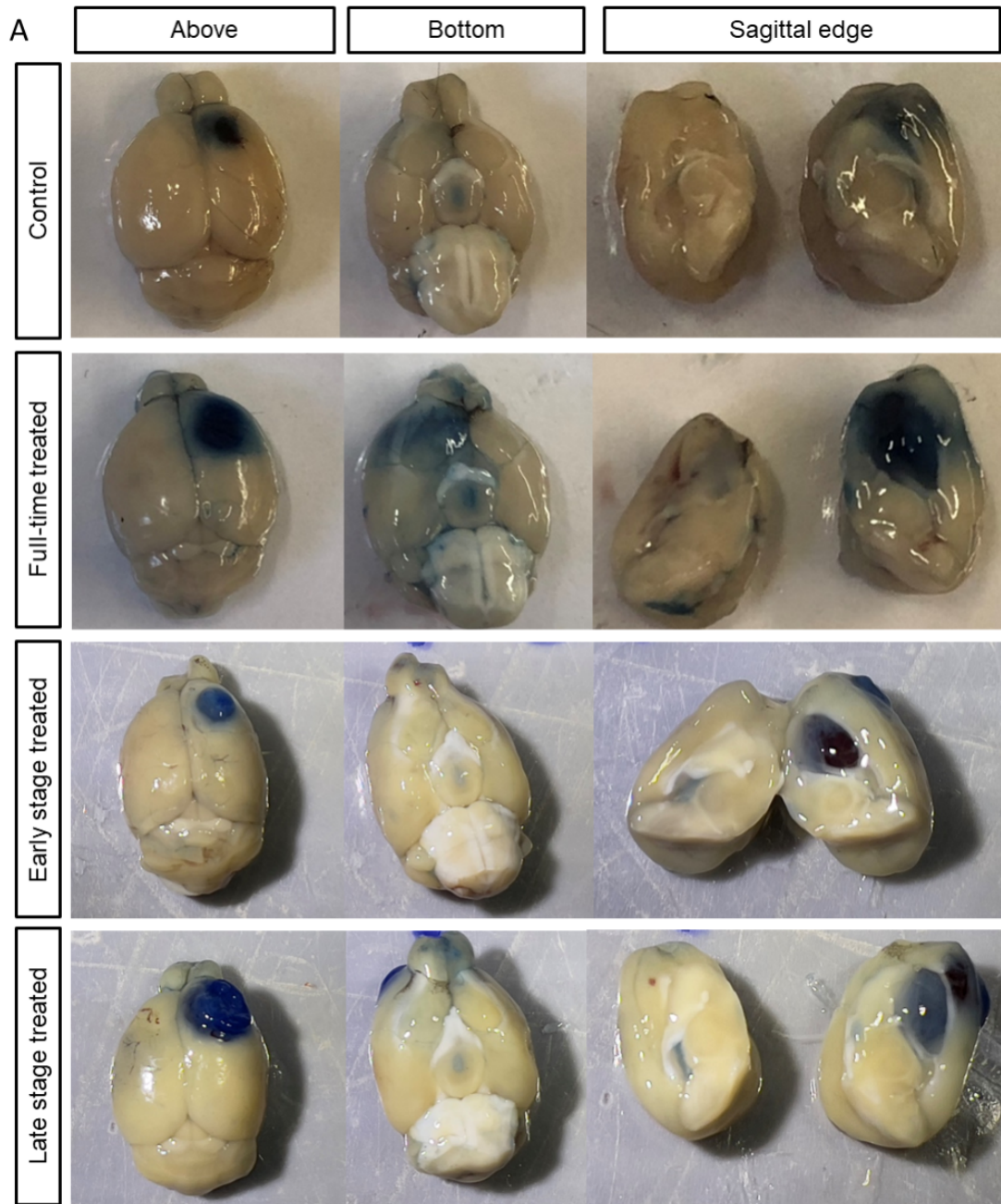


Figure 13 | Full-time BAPN treatment up-regulated Evans blue leakiness in tumor parenchyma

(A) Representative images of Evans blue injected mice brain samples from control and all BAPN treated groups present general Evans blue leakiness sample appearance from the top and bottom positions and vision after cut with sagittal midline. (B) Vascular permeability of the Evans Blue dye extravasation is expressed as $\mu\text{g/g}$ of brain samples. (C) Normalised vascular permeability of the Evans Blue dye extravasation is shown as $\mu\text{g}/\text{mm}^3$ of the tumor. Statistical significance according to one-way ANOVA with post-hoc test is expressed as ** $P < 0.01$, *** $P < 0.001$. Each dot shows the average data acquired from a single mouse. Values are presented as mean \pm SD.

4.3.3 Full-time BAPN treatment aggravated dextran leakiness in tumor parenchyma

70kDa biotin dextran was injected into mice through the tail vein before sacrifice to measure tumor vascular permeability. Dextran leakiness was measured in immunostained mouse brain slices using the ImageJ software (Fig 14A). The results showed that dextran leakage in the tumor parenchyma was significantly higher in full-time-treated mice than in control mice (Fig 14B). Combined with the EB extravasation results, the full-time BAPN treatment improved BTB permeability.

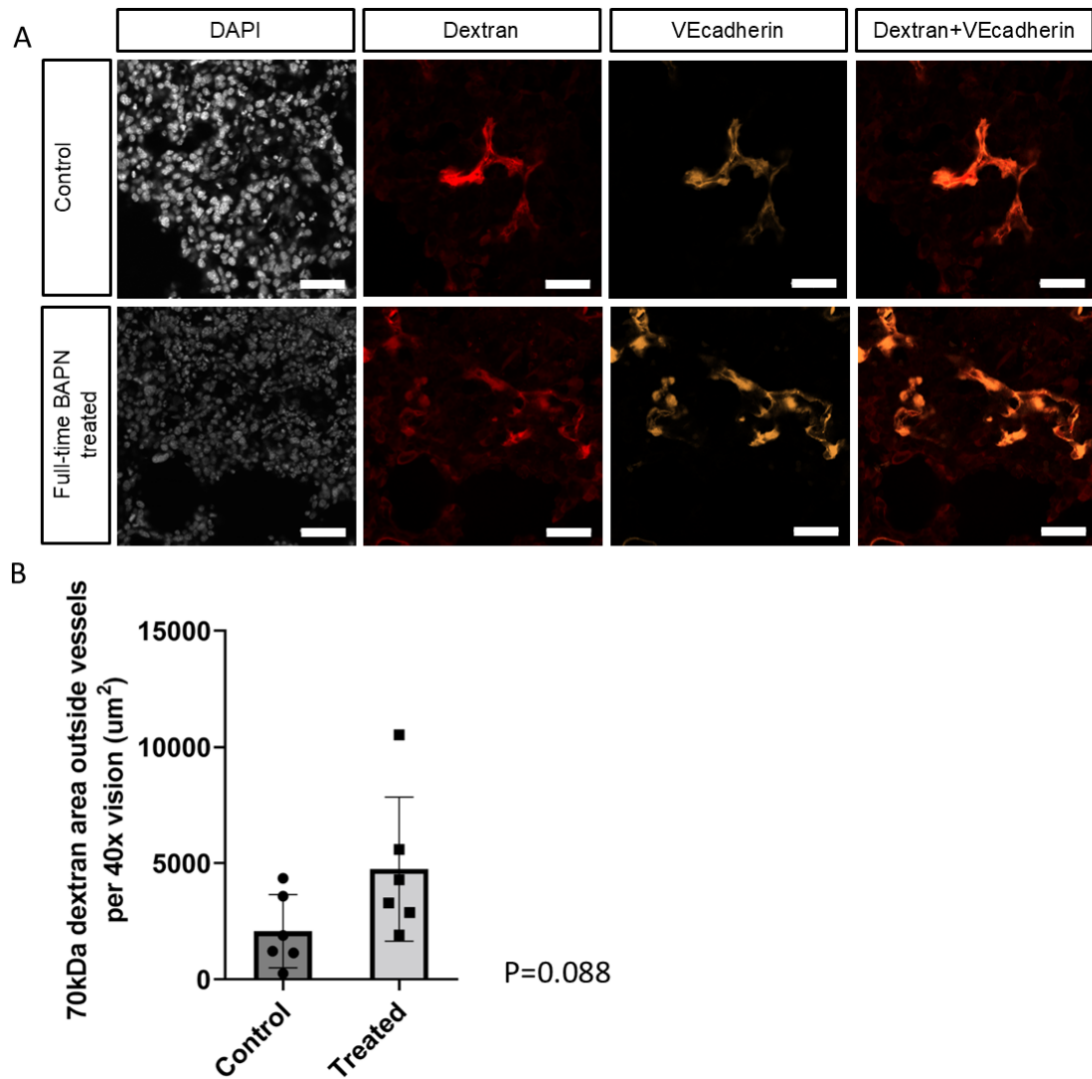


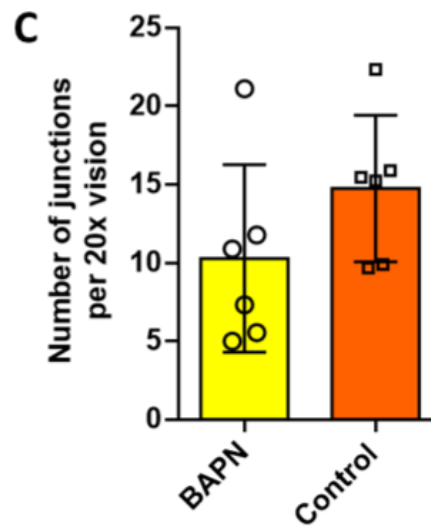
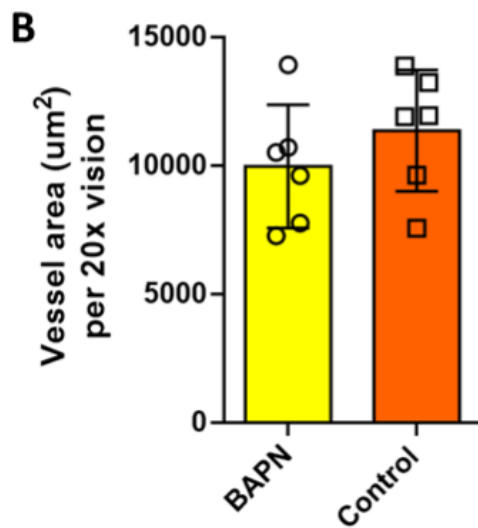
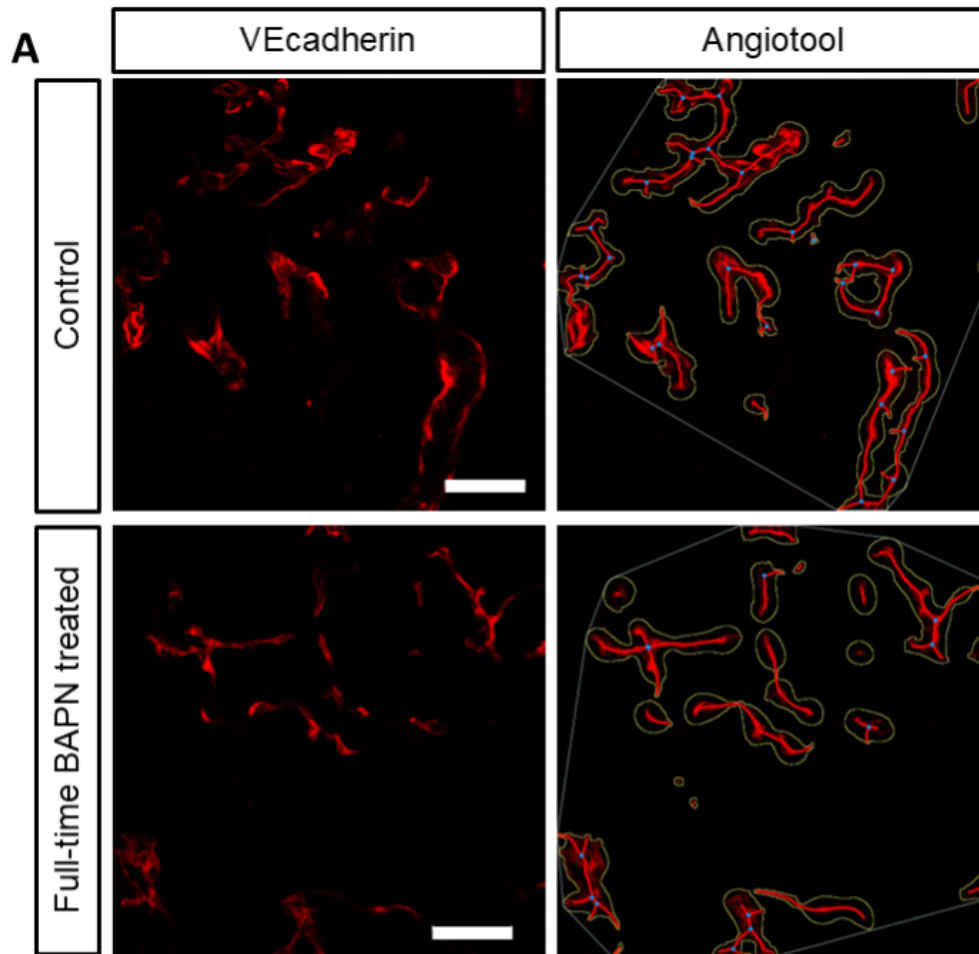
Figure 14 | Full-time BAPN treatment aggravated dextran leakiness in tumor parenchyma

(A) Representative images of 70kDa biotin-dextran and vWF staining of mice from control and full-time BAPN treatment groups. (B) Dextran leakiness results of both groups, $P = 0.08$. Each dot shows the average data acquired from a single mouse. Values are presented as mean \pm SD. Scale bar = 50 μ m.

4.3.4 Full-time BAPN treatment did not affect the angiogenesis in GBM

Because BAPN has a profound effect on the homeostasis of the vessel basement

membrane in GBM, whether BAPN treatment could interfere with tumor angiogenesis in GBM was investigated in this part. The previously mentioned AngioTool software was used to analyse the tumor vasculature (Fig 15A). The results showed no significant differences in the vessel patterns between the control and treated groups (Fig 15B-E).



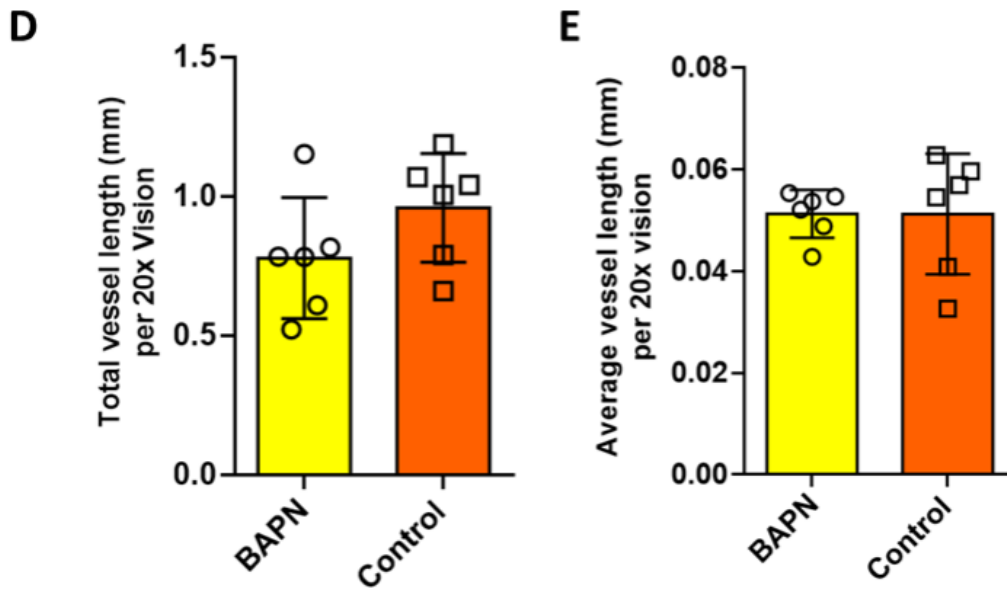


Figure 15 | Full-time BAPN treatment did not obviously affect the angiogenesis in glioblastoma

(A) Representative images of vessel segments and AngioTool analysis. (B) Results of vessel area parameters in AngioTool vasculature analysis. (C) Junction numbers parameters in AngioTool vasculature analysis. (D) Results of total vessel length in AngioTool vasculature analysis. (E) Results of average vessel length parameters in AngioTool vasculature analysis. Statistical significance according to one-way ANOVA with post-hoc test is expressed as * $P < 0.05$. Each dot shows the average data acquired from a single mouse. Values are presented as mean \pm SD. Scale bar = 100 μ m.

5 Discussion

Glioblastoma is one of the most common malignancies in the central nervous system (CNS) in adults. Most patients would still develop fatal recurrent tumors even accepted aggressive treatment including surgical dissection, chemotherapy and radiotherapy, biological treatment, and tumor-treating fields. Platelet-derived growth factors (PDGFs) were found significant in the context of glioblastoma[153]. In the induced GBM mouse models in this research, the PDGFA and PDGFB overexpression subtypes showed shorter survival time than controls. Previous studies have demonstrated that PDGFA and its receptor PDGFRB are overexpressed in glioblastoma (GBM)[153]. They are crucial for maintaining the self-renewal and tumorigenicity of glioma stem cells (GSCs), thus promoting tumorigenesis and leading to shorter lifespans for tumor bearers[154]. The introduction of PDGFB into mice brains has been shown to lead to glioblastoma formation, this effect is enhanced when tumor suppressors like *TP53* and *PTEN* are mutated[155-157]. Moreover, PDGFB-driven GBM has been shown to have extensive interactions with the tumor microenvironment (TME), particularly with tumor-associated macrophages (TAMs)[157, 158]. These interactions further support tumorigenesis through various mechanisms, such as the secretion of pro-inflammatory factors, which enhance tumor-promoting inflammation[157, 158].

Pericytes play a vital role in the pathological progression of GBM, including tumorigenesis, GBM invasion, facilitate the escape of tumor cells from immune surveillance, especially tumor angiogenesis, and blood-tumor barrier (BTB) formation

[110]. Pericytes in GBMs originate from GSCs and from endogenous, physiological pericytes of the brain parenchyma [99, 159]. Communication between pericytes and endothelial cells (ECs) including physical contact and reciprocal paracrine signalling maintains the function and integrity of tumor vessels[160-162]. Previous research proved that vessels with less pericytes coverage were vulnerable to radiation and chemotherapy and demonstrated that pericytes are critical to protect ECs and to promote therapeutic resistance[160, 163]. These features made pericytes a promising target for the GBM treatment. Previous studies have extensively focused on the tumor-derived pericytes population and revealed their function in the BTB and tumorigenesis [99, 159]. Cheng et al found that glioblastoma stem cells (GSCs) generated vascular pericytes support vessel function, tumor growth and were involved in therapeutic resistance[99]. Zhou et al eliminated GSC-derived pericytes in xenograft models and showed that disrupted BTB and increased vascular permeability. This procedure increased the accumulation of chemotherapeutics with poor BTB penetration into the tumor parenchyma and enhanced chemotherapeutic efficacy[159]. However, detailed knowledge on the function of endogenous pericytes in GBMs is lacking. Therefore, the role of endogenous pericytes in GBM drew my attention and prompted me to investigate the potential functions of endogenous pericytes in GBM vasculature.

First, to confirm the origin of pericytes in the GBM vasculature, a range of lineage-tracing mouse GBM models were induced to recapitulate distinct human GBM subtypes. These included different AAVs injected into p53^{fl/fl}/PTEN^{fl/fl}/NF1^{fl/fl} mice

(AAV1/2 cre, p53^{KO}/Pten^{KO}/Nf1^{KO}, tdTomato; AAV1/2 PDGFA-cre p53^{KO}/Pten^{KO}/Nf1^{KO}, tdTomato and AAV1/2 PDGFB-cre, p53^{KO}/Pten^{KO}/Nf1^{KO}, tdTomato), and different transgenic tumor cell lines generated from neural precursor cells (NPCs) extracted from a mouse genotyped p53^{fl/fl}/PTEN^{fl/fl}/NF1^{fl/fl} mouse strains that were transfected with lentivirus containing cre-GFP or PDGFB-cre-GFP. These transgenic tumor models have the same genotype as the AAV-induced models. In the AAV-induced p53^{KO}/Pten^{KO}/Nf1^{KO} models, pericyte coverage fractions were calculated using the ImageJ software. PDGFA or PDGFB overexpression showed no significant upregulation of pericyte coverage compared to controls. Immunofluorescence inspection revealed similar ratios of tumor-derived and endogenous pericytes in all AAV-induced GBM models. Orthotopical implantation of transgenic tumors showed the same trend; host or tumor-derived pericytes accounted for approximately 50% of all pericytes, which is consistent with the AAV-induced p53^{KO}/Pten^{KO}/Nf1^{KO} tumor models. In addition, AAVs were used in CDKN2aKO, p53^{fl/fl}/PTEN^{fl/fl}/NF1^{fl/fl} and stop-tdTomato mice to induce other human GBM subtypes (AAV1/2-PDGFA-cre, CDKN2aKO, p53^{KO}/Pten^{KO}/Nf1^{KO}, tdTomato, AAV1/2-PDGFB-cre, CDKN2aKO, p53^{KO}/Pten^{KO}/Nf1^{KO}, tdTomato). Again, the ratio of tumor-derived and endogenous pericytes was roughly 50:50. These results confirmed that pericytes in GBM originate from different sources, including GSCs and the parenchyma. Furthermore, these experiments revealed that the ratio of tumor-derived pericytes to endogenous pericytes was 1:1, highlighting the importance of endogenous pericytes in GBM.

Previous studies have verified pericyte recruitment as a key step in tumor angiogenesis[100, 113-115]. Pericytes are recruited by the newly sprouted ECs to wrap around the newly formed tube-like vessel structure, stabilise the vessel wall, and eventually form a complete vessel structure [113-115]. AngioTool software, which gave us the ability to measure several morphological and spatial parameters of vessels including the area covered by a vascular network, the number of vessel junctions, total and average vessel length[164], has been used by other investigators to measure vascular patterning [165-168]. Different parameters in AngioTool software represent different vasculature features, vessel area represents vessel density, vessel junction numbers represent the number of branching points, total vessel length represents extent of vessel network and average vessel length represents the mean length of individual vessel segments [164]. All these parameters reflect the status of angiogenesis and maturation of newly formed vessels, helped to evaluate if the newly generated vessel network has full functions[164]. The vessel area results showed mainly in tumor-core area the vessel density varies a lot among GBMs with different driver mutations. But roughly the PDGFB overexpressing GBM shows higher vessel density than other GBM subtypes. While AAV-PDGFB p53/Pten/Nf1 KO model showed higher vessel density than implanted p53/Pten/Nf1 KO and AAV-PDGFA Cdkn2aKO models in tumor invasive area. The junction numbers result showed in the tumor core area, the branching points number significantly varies among different GBM subtypes, roughly non-overexpression models had highest numbers. Meanwhile only a few significances were observed in tumor invasive area, AAV-PDGFA p53/Pten/Nf1 KO model shows higher

junction numbers than AAV-PDGFB p53/Pten/Nf1 KO and implanted p53/Pten/Nf1 KO models. In tumor core area in total vessel length result, the extent of tumor vessels hugely varies among GBM with different driver mutations. In tumor invasive area, AAV-cre p53/Pten/Nf1 KO model showed higher parameters than in AAV-PDGFA Cdkn2aKO model; AAV-PDGFA p53/Pten/Nf1 KO model showed higher parameters than AAV-PDGFA Cdkn2aKO model. At last, in average vessel length area parameter, only in tumor core significant differences were observed among different GBM subtypes. Previous research has indicated that PDGFs play crucial roles in promoting tumor angiogenesis, particularly by recruiting pericytes and enhancing vessel maturation [157, 169]. In this study on vasculature, the overexpression of PDGFA and PDGFB were found significantly impacted tumor vasculature maturation, primarily within the tumor core area. Models with PDGFs overexpression generally exhibited increased vessel density, fewer junctions, and a reduced average vessel length compared to non-expressing models, characteristics indicative of mature vessel networks [170]. Overall, this study demonstrates that vascular patterning varies substantially among different tumor models and suggests that PDGF overexpression promotes angiogenesis in GBM.

Considering the important role of pericytes in maintaining the integrity of the BBB [97], I wondered if these could be targeted in GBM to improve treatment efficacy and prognosis. GBM is a CNS malignancy with several distinguishing features including extremely rapid progression and recurrence [2, 5, 6]. Most patients with primary GBMs

can only be diagnosed when the tumor is already considerably advanced. After tumor resection, regular brain examinations in GBM patients may enable early detection of recurrent GBM. However, treatment of relapsing GBM is challenging. Only 50% patients are eligible for second surgery. Reirradiation and temozolomide rechallenging show mild clinical benefit compared to best supportive care, other treatment like anti-angiogenic treatment and tumor treating fields have no efficacy in randomized trials [171]. One theory for the point of origin of glioblastoma relapse is that recurrent GBM may arise from tumor cells that survived systematic treatment. Here, the BTB prevents chemotherapeutic drugs from accumulating in some parts of the tumor parenchyma. These phenomena have drawn my attention and prompted me to investigate whether pericytes can be targeted at early stages of relapsing GBMs in order to modulate the BTB and to improve treatment efficacy.

With this hypothesis, a transgenic mouse host GBM cell line GL261-HSVTK was injected into conditional pericyte ablated mice (PDGFRB-iDTA) to induce relapse GBM mice models. Different pericyte-depletion schemes were applied (early and late stages) to investigate the effects of different ablation time points. Dextran leakiness analysis revealed that early ablation of pericytes could significantly upregulate vessel permeability compared to controls and late-depleted tumors. However, in the vasculature analysis, no significant differences were observed in any of the parameters between the control, early-, and late-depleted groups. These results demonstrate the important role of pericytes in maintaining the integrity of the BTB, which is also

consistent with previous results showing that pericytes did not control the morphology of tumor vasculature. More importantly, these findings suggest that pericytes are promising therapeutic targets for recurrent GBMs, but only after treatment is started at an early stage after first-line therapy.

Angiogenesis is a central feature of glioblastoma, the basement membrane plays a crucial role in the structure and functions tumor blood vessels. The basement membrane is made of several components including collagens, laminins, nidogens and perlecan [172]. Crosslinking of elastin and collagens in basement membrane maintains the integrity of the blood-brain barrier[119]. A large number of studies have focused on the anti-angiogenic treatment of GBM, including vascular endothelial growth factor (VEGF) inhibition[173], anti-angiogenic agents combined with other treatments[174], alternative angiogenic pathways beyond VEGF [100] and novel agents[175]. But unfortunately, anti-angiogenic treatment has limited effects [34-36]. Bevacizumab, a monoclonal antibody targeting VEGF, is the most common anti-angiogenic drug used in clinical treatment of GBM approved by the FDA. It can reduce edema and improve progression-free survival, but showed no significant improvement on overall survival[173]. Bevacizumab was also applied combined with temozolomide and radiotherapy in some studies, but has shown limited effects[174]. Other studies focused on angiogenic pathways beyond VEGF, such as angiopoietins, fibroblast growth factors (FGFs), and platelet-derived growth factors (PDGFs), also showed unclear efficacy[100]. In this study, pericyte-targeted treatment was achieved in transgenic mice.

Lysyl oxidases (LOX) expression was upregulated by hypoxia induce factor 1 (HIF-1) in the newly formed vessels in glioblastoma, enhancing the crosslinking of elastin and collagens in the basement membrane and maintaining the integrity and function of BBB[125]. Meanwhile, LOX expression in tumor-free tissues remained at a very low level[125]. This feature led to the hypothesis that LOX may be considered a potential tumor-specific therapeutic target to breakdown the BTB and improve the chemotherapy efficacy. BAPN, a natural toxin, which is an inhibitor of lysyl oxidases (LOX), can suppress the form of crosslinking between extracellular matrix components like elastin and collagens in basement membrane of blood vessels, came into my sight [138, 140]. In this study, a range of wild-type mice implanted with mouse host GBM cells were induced and treated with BAPN in drinking water at different time points (full-time, early treatment, and late treatment). Mice treated during the whole tumor progression period showed smaller tumors compared to controls and both part-time-treated (early and late) groups, while part-time treatment no matter early or late tumor stages showed no obvious significant difference compared to controls, suggesting that full-time BAPN treatment could suppress tumorigenesis. Evans blue assay results showed that full-time BAPN treatment could augment leakiness compared with the other groups. Moreover, when Evans blue leakage was normalised to the average tumor size in each group, the smaller tumors from full-time treated group even showed higher leakiness than other groups with bigger tumors, suggesting BAPN could modulate the BTB and upregulate the permeability of BTB. In the dextran leakiness analysis, the full-time treated group showed significantly higher leakage than the other groups, which was consistent with

the results of the EB assays. This experiment suggests that full-time BAPN treatment can disrupt the BTB and improve chemotherapy efficacy. However, only full-time BAPN showed anti-angiogenic treatment efficacy, whereas part-time treatment, regardless of early or late stage, exerted no therapeutic effects. A potential explanation for why only full-time application of BAPN shows treatment efficacy could be that BAPN needs extended ingestion periods to accumulate to effective concentrations within the tumor to effectively block the crosslinking of the extracellular matrix (ECM) in the basement membrane[176].

In this study, the lineage-tracing capacity of a range of transgenic GBM mouse models were leveraged, recapitulating distinct human GBM subtypes, to identify and quantify the contribution of tumor- or host-derived mural cells to the neoplastic vasculature. These models allow the exact classification of the mural cell origin and reveal a profound and stable contribution of host-derived pericytes to GBM vessels [177]. Vascular patterning was found to vary among GBM with different driver mutations. Surprisingly, the host and tumor were found equally generated a population of intratumoral vascular mural cells, without any dependence on the GBM subtype. Moreover, this study revealed that targeting pericytes could break down the BTB, thereby potentially improving treatment efficacy. Overall, this research suggests that tumor parenchymal pericytes are therapeutically promising targets for BTB modulation and improved GBM treatment.

References

1. Wu, F., et al., *Prognostic power of a lipid metabolism gene panel for diffuse gliomas*. J Cell Mol Med, 2019. **23**(11): p. 7741-7748.
2. Ostrom, Q.T., et al., *CBTRUS Statistical Report: Primary Brain and Other Central Nervous System Tumors Diagnosed in the United States in 2014-2018*. Neuro Oncol, 2021. **23**(12 Suppl 2): p. iii1-iii105.
3. Louis, D.N., et al., *The 2021 WHO Classification of Tumors of the Central Nervous System: a summary*. Neuro Oncol, 2021. **23**(8): p. 1231-1251.
4. Wen, P.Y., et al., *Glioblastoma in adults: a Society for Neuro-Oncology (SNO) and European Society of Neuro-Oncology (EANO) consensus review on current management and future directions*. Neuro Oncol, 2020. **22**(8): p. 1073-1113.
5. Mohammed, S., M. Dinesan, and T. Ajayakumar, *Survival and quality of life analysis in glioblastoma multiforme with adjuvant chemoradiotherapy: a retrospective study*. Rep Pract Oncol Radiother, 2022. **27**(6): p. 1026-1036.
6. Batash, R., et al., *Glioblastoma Multiforme, Diagnosis and Treatment; Recent Literature Review*. Curr Med Chem, 2017. **24**(27): p. 3002-3009.
7. Schaff, L.R. and I.K. Mellinghoff, *Glioblastoma and Other Primary Brain Malignancies in Adults: A Review*. JAMA, 2023. **329**(7): p. 574-587.
8. Ohgaki, H. and P. Kleihues, *The definition of primary and secondary glioblastoma*. Clin Cancer Res, 2013. **19**(4): p. 764-72.
9. Nobusawa, S., et al., *IDH1 mutations as molecular signature and predictive factor of secondary glioblastomas*. Clin Cancer Res, 2009. **15**(19): p. 6002-7.
10. Balss, J., et al., *Analysis of the IDH1 codon 132 mutation in brain tumors*. Acta Neuropathol, 2008. **116**(6): p. 597-602.
11. Hartmann, C., et al., *Patients with IDH1 wild type anaplastic astrocytomas exhibit worse prognosis than IDH1-mutated glioblastomas, and IDH1 mutation status accounts for the unfavorable prognostic effect of higher age: implications for classification of gliomas*. Acta Neuropathol, 2010. **120**(6): p. 707-18.

12. Neftel, C., et al., *An Integrative Model of Cellular States, Plasticity, and Genetics for Glioblastoma*. Cell, 2019. **178**(4): p. 835-849 e21.
13. Verhaak, R.G., et al., *Integrated genomic analysis identifies clinically relevant subtypes of glioblastoma characterized by abnormalities in PDGFRA, IDH1, EGFR, and NF1*. Cancer Cell, 2010. **17**(1): p. 98-110.
14. Hovinga, K.E., et al., *EGFR amplification and classical subtype are associated with a poor response to bevacizumab in recurrent glioblastoma*. J Neurooncol, 2019. **142**(2): p. 337-345.
15. Olar, A. and K.D. Aldape, *Using the molecular classification of glioblastoma to inform personalized treatment*. J Pathol, 2014. **232**(2): p. 165-77.
16. Kuriakose, N., et al., *Characterization of Rh-Al Bond in Rh(PAIP) (PAIP = Pincer-type Diphosphino-Aluminyll Ligand) in Comparison with Rh(L)(PMe(3))(2) (L = AlMe(2), Al(NMe(2))(2), BR(2), SiR(3), CH(3), Cl, or OCH(3)): Theoretical Insight*. Inorg Chem, 2019. **58**(8): p. 4894-4906.
17. Tran, A.N. and C. Horbinski, *Mesenchymal stemlike cells in glioblastoma*. Neuro Oncol, 2020. **22**(10): p. 1409-1410.
18. Behnan, J., G. Finocchiaro, and G. Hanna, *The landscape of the mesenchymal signature in brain tumors*. Brain, 2019. **142**(4): p. 847-866.
19. Alessandrini, F., et al., *Glioblastoma models driven by different mutations converge to the proneural subtype*. Cancer Lett, 2020. **469**: p. 447-455.
20. Sidaway, P., *CNS cancer: Glioblastoma subtypes revisited*. Nat Rev Clin Oncol, 2017. **14**(10): p. 587.
21. Weller, M., et al., *Standards of care for treatment of recurrent glioblastoma--are we there yet?* Neuro Oncol, 2013. **15**(1): p. 4-27.
22. Weller, M. and E. Le Rhun, *How did lomustine become standard of care in recurrent glioblastoma?* Cancer Treat Rev, 2020. **87**: p. 102029.
23. Audureau, E., et al., *Prognostic factors for survival in adult patients with recurrent glioblastoma: a decision-tree-based model*. J Neurooncol, 2018. **136**(3): p. 565-576.
24. Piper, R.J., et al., *Neuroimaging classification of progression patterns in*

- glioblastoma: a systematic review.* J Neurooncol, 2018. **139**(1): p. 77-88.
25. Bordignon, K.C., et al., *Patterns of neuroaxis dissemination of gliomas: suggestion of a classification based on magnetic resonance imaging findings.* Surg Neurol, 2006. **65**(5): p. 472-7; discussion 477.
 26. Woodroffe, R.W., et al., *Survival after reoperation for recurrent glioblastoma.* J Clin Neurosci, 2020. **73**: p. 118-124.
 27. Helseth, R., et al., *Overall survival, prognostic factors, and repeated surgery in a consecutive series of 516 patients with glioblastoma multiforme.* Acta Neurol Scand, 2010. **122**(3): p. 159-67.
 28. Barbagallo, G.M., M.D. Jenkinson, and A.R. Brodbelt, *'Recurrent' glioblastoma multiforme, when should we reoperate?* Br J Neurosurg, 2008. **22**(3): p. 452-5.
 29. Shi, W., et al., *Investigating the Effect of Reirradiation or Systemic Therapy in Patients With Glioblastoma After Tumor Progression: A Secondary Analysis of NRG Oncology/Radiation Therapy Oncology Group Trial 0525.* Int J Radiat Oncol Biol Phys, 2018. **100**(1): p. 38-44.
 30. Perry, J.R., et al., *Phase II trial of continuous dose-intense temozolomide in recurrent malignant glioma: RESCUE study.* J Clin Oncol, 2010. **28**(12): p. 2051-7.
 31. Pedersen, P.B., et al., *Prevalence and prognosis of acutely ill patients with organ failure at arrival to hospital: protocol for a systematic review.* Syst Rev, 2017. **6**(1): p. 227.
 32. Stupp, R., et al., *NovoTTF-100A versus physician's choice chemotherapy in recurrent glioblastoma: a randomised phase III trial of a novel treatment modality.* Eur J Cancer, 2012. **48**(14): p. 2192-202.
 33. Lombardi, G., et al., *Regorafenib compared with lomustine in patients with relapsed glioblastoma (REGOMA): a multicentre, open-label, randomised, controlled, phase 2 trial.* Lancet Oncol, 2019. **20**(1): p. 110-119.
 34. Lee, E.Q., et al., *Phase II study of panobinostat in combination with bevacizumab for recurrent glioblastoma and anaplastic glioma.* Neuro Oncol, 2015. **17**(6): p. 862-7.

35. Xu, Q., et al., *Safety and Efficacy of Anlotinib Hydrochloride Plus Temozolomide in Patients with Recurrent Glioblastoma*. Clin Cancer Res, 2023. **29**(19): p. 3859-3866.
36. Yin, J., et al., *Anlotinib as Monotherapy or Combination Therapy for Recurrent High-Grade Glioma: A Retrospective Study*. Clin Med Insights Oncol, 2023. **17**: p. 11795549231175714.
37. Zhang, H., *A study on the control of vascular permeability in GBM. The role of pericytes, myeloid-like cells (TAMEP) and the angiogenic factors APLN and ANGPT2.*, Dissertation, LMU Munich. 2021, LMU Munich.
38. Takanashi, N., et al., *Generation and measurement of a squeezed vacuum up to 100 MHz at 1550 nm with a semi-monolithic optical parametric oscillator designed towards direct coupling with waveguide modules*. Opt Express, 2019. **27**(13): p. 18900-18909.
39. Takano, S., T. Yamashita, and O. Ohneda, *Molecular therapeutic targets for glioma angiogenesis*. J Oncol, 2010. **2010**: p. 351908.
40. Ahir, B.K., H.H. Engelhard, and S.S. Lakka, *Tumor Development and Angiogenesis in Adult Brain Tumor: Glioblastoma*. Mol Neurobiol, 2020. **57**(5): p. 2461-2478.
41. Yasuno, K., et al., *Common variant near the endothelin receptor type A (EDNRA) gene is associated with intracranial aneurysm risk*. Proc Natl Acad Sci U S A, 2011. **108**(49): p. 19707-12.
42. Liao, D. and R.S. Johnson, *Hypoxia: a key regulator of angiogenesis in cancer*. Cancer Metastasis Rev, 2007. **26**(2): p. 281-90.
43. Gonzalez-Avila, G., et al., *Hypoxic Effects on Matrix Metalloproteinases' Expression in the Tumor Microenvironment and Therapeutic Perspectives*. Int J Mol Sci, 2023. **24**(23).
44. Fitsialos, G., et al., *HIF1 transcription factor regulates laminin-332 expression and keratinocyte migration*. J Cell Sci, 2008. **121**(Pt 18): p. 2992-3001.
45. Wise, D.R., et al., *Hypoxia promotes isocitrate dehydrogenase-dependent carboxylation of alpha-ketoglutarate to citrate to support cell growth and*

- viability*. Proc Natl Acad Sci U S A, 2011. **108**(49): p. 19611-6.
46. Stacker, S.A., et al., *VEGF-D promotes the metastatic spread of tumor cells via the lymphatics*. Nat Med, 2001. **7**(2): p. 186-91.
 47. Yang, Y., et al., *Cancer stem cells and angiogenesis*. Pathol Res Pract, 2024. **253**: p. 155064.
 48. Rifkin, D.B. and D. Moscatelli, *Recent developments in the cell biology of basic fibroblast growth factor*. J Cell Biol, 1989. **109**(1): p. 1-6.
 49. Suri, C., et al., *Increased vascularization in mice overexpressing angiopoietin-1*. Science, 1998. **282**(5388): p. 468-71.
 50. Gleave, M.E., et al., *Epidermal growth factor receptor-mediated autocrine and paracrine stimulation of human transitional cell carcinoma*. Cancer Res, 1993. **53**(21): p. 5300-7.
 51. Lakka, S.S. and J.S. Rao, *Antiangiogenic therapy in brain tumors*. Expert Rev Neurother, 2008. **8**(10): p. 1457-73.
 52. Senger, D.R. and G.E. Davis, *Angiogenesis*. Cold Spring Harb Perspect Biol, 2011. **3**(8): p. a005090.
 53. Khodadust, F., et al., *Systematic Review: Targeted Molecular Imaging of Angiogenesis and Its Mediators in Rheumatoid Arthritis*. Int J Mol Sci, 2022. **23**(13).
 54. Ameratunga, M., et al., *Anti-angiogenic therapy for high-grade glioma*. Cochrane Database Syst Rev, 2018. **11**(11): p. CD008218.
 55. Shikalov, A., I. Koman, and N.M. Kogan, *Targeted Glioma Therapy-Clinical Trials and Future Directions*. Pharmaceutics, 2024. **16**(1).
 56. Ahluwalia, M.S. and C.L. Gladson, *Progress on antiangiogenic therapy for patients with malignant glioma*. J Oncol, 2010. **2010**: p. 689018.
 57. O'Brown, N.M., S.J. Pfau, and C. Gu, *Bridging barriers: a comparative look at the blood-brain barrier across organisms*. Genes Dev, 2018. **32**(7-8): p. 466-478.
 58. Abbott, N.J., *Blood-brain barrier structure and function and the challenges for CNS drug delivery*. J Inherit Metab Dis, 2013. **36**(3): p. 437-49.

59. Sharma, A., et al., *Nanowired Drug Delivery Across the Blood-Brain Barrier in Central Nervous System Injury and Repair*. *CNS Neurol Disord Drug Targets*, 2016. **15**(9): p. 1092-1117.
60. Sharma, H.S., J. Westman, and F. Nyberg, *Pathophysiology of brain edema and cell changes following hyperthermic brain injury*. *Prog Brain Res*, 1998. **115**: p. 351-412.
61. Kiyatkin, E.A. and H.S. Sharma, *Leakage of the blood-brain barrier followed by vasogenic edema as the ultimate cause of death induced by acute methamphetamine overdose*. *Int Rev Neurobiol*, 2019. **146**: p. 189-207.
62. Matsumoto, J., et al., *The Transport Mechanism of Extracellular Vesicles at the Blood-Brain Barrier*. *Curr Pharm Des*, 2017. **23**(40): p. 6206-6214.
63. Lu, W., *Adsorptive-mediated brain delivery systems*. *Curr Pharm Biotechnol*, 2012. **13**(12): p. 2340-8.
64. Arvanitis, C.D., G.B. Ferraro, and R.K. Jain, *The blood-brain barrier and blood-tumor barrier in brain tumors and metastases*. *Nat Rev Cancer*, 2020. **20**(1): p. 26-41.
65. Nation, D.A., et al., *Blood-brain barrier breakdown is an early biomarker of human cognitive dysfunction*. *Nat Med*, 2019. **25**(2): p. 270-276.
66. Sweeney, M.D., et al., *Blood-Brain Barrier: From Physiology to Disease and Back*. *Physiol Rev*, 2019. **99**(1): p. 21-78.
67. Choudhury, H., et al., *Transferrin receptors-targeting nanocarriers for efficient targeted delivery and transcytosis of drugs into the brain tumors: a review of recent advancements and emerging trends*. *Drug Deliv Transl Res*, 2018. **8**(5): p. 1545-1563.
68. Pulgar, V.M., *Transcytosis to Cross the Blood Brain Barrier, New Advancements and Challenges*. *Front Neurosci*, 2018. **12**: p. 1019.
69. Sharma, H.S., *Pathophysiology of blood-spinal cord barrier in traumatic injury and repair*. *Curr Pharm Des*, 2005. **11**(11): p. 1353-89.
70. Sarkaria, J.N., et al., *Is the blood-brain barrier really disrupted in all glioblastomas? A critical assessment of existing clinical data*. *Neuro Oncol*,

2018. **20**(2): p. 184-191.
71. van Tellingen, O., et al., *Overcoming the blood-brain tumor barrier for effective glioblastoma treatment*. Drug Resist Updat, 2015. **19**: p. 1-12.
72. Dubois, L.G., et al., *Gliomas and the vascular fragility of the blood brain barrier*. Front Cell Neurosci, 2014. **8**: p. 418.
73. Pitz, M.W., et al., *Tissue concentration of systemically administered antineoplastic agents in human brain tumors*. J Neurooncol, 2011. **104**(3): p. 629-38.
74. Schaffenrath, J., et al., *Blood-brain barrier alterations in human brain tumors revealed by genome-wide transcriptomic profiling*. Neuro Oncol, 2021. **23**(12): p. 2095-2106.
75. Haumann, R., et al., *Overview of Current Drug Delivery Methods Across the Blood-Brain Barrier for the Treatment of Primary Brain Tumors*. CNS Drugs, 2020. **34**(11): p. 1121-1131.
76. Winkler, E.A., R.D. Bell, and B.V. Zlokovic, *Central nervous system pericytes in health and disease*. Nat Neurosci, 2011. **14**(11): p. 1398-1405.
77. Attwell, D., et al., *What is a pericyte?* J Cereb Blood Flow Metab, 2016. **36**(2): p. 451-5.
78. Hartmann, D.A., et al., *Pericyte structure and distribution in the cerebral cortex revealed by high-resolution imaging of transgenic mice*. Neurophotonics, 2015. **2**(4): p. 041402.
79. Daneman, R., et al., *Pericytes are required for blood-brain barrier integrity during embryogenesis*. Nature, 2010. **468**(7323): p. 562-6.
80. Armulik, A., G. Genove, and C. Betsholtz, *Pericytes: developmental, physiological, and pathological perspectives, problems, and promises*. Dev Cell, 2011. **21**(2): p. 193-215.
81. Bell, R.D., et al., *Pericytes control key neurovascular functions and neuronal phenotype in the adult brain and during brain aging*. Neuron, 2010. **68**(3): p. 409-27.
82. Zhao, Z., et al., *Establishment and Dysfunction of the Blood-Brain Barrier*. Cell,

2015. **163**(5): p. 1064-1078.
83. Armulik, A., et al., *Pericytes regulate the blood-brain barrier*. Nature, 2010. **468**(7323): p. 557-61.
84. Fu, J., et al., *Brain pericyte biology: from physiopathological mechanisms to potential therapeutic applications in ischemic stroke*. Front Cell Neurosci, 2023. **17**: p. 1267785.
85. Benarroch, E., *What Are the Roles of Pericytes in the Neurovascular Unit and Its Disorders?* Neurology, 2023. **100**(20): p. 970-977.
86. Siekmann, A.F., *Biology of vascular mural cells*. Development, 2023. **150**(16).
87. Wu, Y., et al., *Biology and function of pericytes in the vascular microcirculation*. Animal Model Exp Med, 2023. **6**(4): p. 337-345.
88. Yu, D., et al., *Myogenic Differentiation of Stem Cells for Skeletal Muscle Regeneration*. Stem Cells Int, 2021. **2021**: p. 8884283.
89. Dabravolski, S.A., et al., *The Role of Pericytes in Regulation of Innate and Adaptive Immunity*. Biomedicines, 2023. **11**(2).
90. Kovac, A., M.A. Erickson, and W.A. Banks, *Brain microvascular pericytes are immunoactive in culture: cytokine, chemokine, nitric oxide, and LRP-1 expression in response to lipopolysaccharide*. J Neuroinflammation, 2011. **8**: p. 139.
91. Jansson, D., et al., *A role for human brain pericytes in neuroinflammation*. J Neuroinflammation, 2014. **11**: p. 104.
92. Nakagomi, T., et al., *Brain vascular pericytes following ischemia have multipotential stem cell activity to differentiate into neural and vascular lineage cells*. Stem Cells, 2015. **33**(6): p. 1962-74.
93. Winkler, E.A., et al., *Blood-spinal cord barrier disruption contributes to early motor-neuron degeneration in ALS-model mice*. Proc Natl Acad Sci U S A, 2014. **111**(11): p. E1035-42.
94. Davalos, D., et al., *Fibrinogen-induced perivascular microglial clustering is required for the development of axonal damage in neuroinflammation*. Nat Commun, 2012. **3**: p. 1227.

95. Jackson, S., et al., *Blood-brain barrier pericyte importance in malignant gliomas: what we can learn from stroke and Alzheimer's disease*. *Neuro Oncol*, 2017. **19**(9): p. 1173-1182.
96. Manandhar, R., et al., *Maternal near miss at Kathmandu Medical College: An analysis of severe maternal morbidity at a Nepalese tertiary care facility*. *Aust N Z J Obstet Gynaecol*, 2023. **63**(4): p. 527-534.
97. Sweeney, M.D., S. Ayyadurai, and B.V. Zlokovic, *Pericytes of the neurovascular unit: key functions and signaling pathways*. *Nat Neurosci*, 2016. **19**(6): p. 771-83.
98. Xian, X., et al., *Pericytes limit tumor cell metastasis*. *J Clin Invest*, 2006. **116**(3): p. 642-51.
99. Cheng, L., et al., *Glioblastoma stem cells generate vascular pericytes to support vessel function and tumor growth*. *Cell*, 2013. **153**(1): p. 139-52.
100. Jain, R.K., et al., *Angiogenesis in brain tumors*. *Nat Rev Neurosci*, 2007. **8**(8): p. 610-22.
101. Zhao, Y., et al., *Stromal cells in the tumor microenvironment: accomplices of tumor progression?* *Cell Death Dis*, 2023. **14**(9): p. 587.
102. Valdor, R., et al., *Glioblastoma progression is assisted by induction of immunosuppressive function of pericytes through interaction with tumor cells*. *Oncotarget*, 2017. **8**(40): p. 68614-68626.
103. Lebeau, G., et al., *Perivascular Mesenchymal Stem/Stromal Cells, an Immune Privileged Niche for Viruses?* *Int J Mol Sci*, 2022. **23**(14).
104. Shi, T., et al., *The Role of Hypoxia and Cancer Stem Cells in Development of Glioblastoma*. *Cancers (Basel)*, 2023. **15**(9).
105. Liebelt, B.D., et al., *Glioma Stem Cells: Signaling, Microenvironment, and Therapy*. *Stem Cells Int*, 2016. **2016**: p. 7849890.
106. Cooke, V.G., et al., *Pericyte depletion results in hypoxia-associated epithelial-to-mesenchymal transition and metastasis mediated by met signaling pathway*. *Cancer Cell*, 2012. **21**(1): p. 66-81.
107. Bentolila, L.A., et al., *Imaging of Angiotropism/Vascular Co-Option in a Murine*

- Model of Brain Melanoma: Implications for Melanoma Progression along Extravascular Pathways*. Sci Rep, 2016. **6**: p. 23834.
108. Ribatti, D. and F. Pezzella, *Vascular Co-Option and Other Alternative Modalities of Growth of Tumor Vasculature in Glioblastoma*. Front Oncol, 2022. **12**: p. 874554.
 109. Sattiraju, A., K.K.S. Sai, and A. Mintz, *Glioblastoma Stem Cells and Their Microenvironment*. Adv Exp Med Biol, 2017. **1041**: p. 119-140.
 110. Sattiraju, A. and A. Mintz, *Pericytes in Glioblastomas: Multifaceted Role Within Tumor Microenvironments and Potential for Therapeutic Interventions*. Adv Exp Med Biol, 2019. **1147**: p. 65-91.
 111. Behling, K., et al., *Remodeling the Vascular Microenvironment of Glioblastoma with alpha-Particles*. J Nucl Med, 2016. **57**(11): p. 1771-1777.
 112. Sattiraju, A., et al., *Alpha Particle Enhanced Blood Brain/Tumor Barrier Permeabilization in Glioblastomas Using Integrin Alpha-v Beta-3-Targeted Liposomes*. Mol Cancer Ther, 2017. **16**(10): p. 2191-2200.
 113. Wu, D., et al., *The blood-brain barrier: structure, regulation, and drug delivery*. Signal Transduct Target Ther, 2023. **8**(1): p. 217.
 114. Mancuso, M.R., et al., *Rapid vascular regrowth in tumors after reversal of VEGF inhibition*. J Clin Invest, 2006. **116**(10): p. 2610-21.
 115. Ribeiro, A.L. and O.K. Okamoto, *Combined effects of pericytes in the tumor microenvironment*. Stem Cells Int, 2015. **2015**: p. 868475.
 116. Lindahl, P., et al., *Pericyte loss and microaneurysm formation in PDGF-B-deficient mice*. Science, 1997. **277**(5323): p. 242-5.
 117. Sugiyama, K., et al., *Pulse-heating ionization for protein on-chip mass spectrometry*. Anal Chem, 2014. **86**(15): p. 7593-7.
 118. Zlokovic, B.V., *The blood-brain barrier in health and chronic neurodegenerative disorders*. Neuron, 2008. **57**(2): p. 178-201.
 119. Xu, L., A. Nirwane, and Y. Yao, *Basement membrane and blood-brain barrier*. Stroke Vasc Neurol, 2019. **4**(2): p. 78-82.
 120. Chitty, J.L., Y.F.I. Setargew, and T.R. Cox, *Targeting the lysyl oxidases in tumor*

- desmoplasia*. Biochem Soc Trans, 2019. **47**(6): p. 1661-1678.
121. Yamauchi, M., et al., *Analysis of collagen and elastin cross-links*. Methods Cell Biol, 2018. **143**: p. 115-132.
 122. Sherman, V.R., W. Yang, and M.A. Meyers, *The materials science of collagen*. J Mech Behav Biomed Mater, 2015. **52**: p. 22-50.
 123. Saini, K., et al., *Tension in fibrils suppresses their enzymatic degradation - A molecular mechanism for 'use it or lose it'*. Matrix Biol, 2020. **85-86**: p. 34-46.
 124. Schmelzer, C.E.H., et al., *Lysyl oxidase-like 2 (LOXL2)-mediated cross-linking of tropoelastin*. FASEB J, 2019. **33**(4): p. 5468-5481.
 125. El-Haibi, C.P., et al., *Critical role for lysyl oxidase in mesenchymal stem cell-driven breast cancer malignancy*. Proc Natl Acad Sci U S A, 2012. **109**(43): p. 17460-5.
 126. Levental, K.R., et al., *Matrix crosslinking forces tumor progression by enhancing integrin signaling*. Cell, 2009. **139**(5): p. 891-906.
 127. Salvador, F., et al., *Lysyl Oxidase-like Protein LOXL2 Promotes Lung Metastasis of Breast Cancer*. Cancer Res, 2017. **77**(21): p. 5846-5859.
 128. Choi, S.K., et al., *LOXL4 knockdown enhances tumor growth and lung metastasis through collagen-dependent extracellular matrix changes in triple-negative breast cancer*. Oncotarget, 2017. **8**(7): p. 11977-11989.
 129. Wu, G., et al., *LOXL1 and LOXL4 are epigenetically silenced and can inhibit ras/extracellular signal-regulated kinase signaling pathway in human bladder cancer*. Cancer Res, 2007. **67**(9): p. 4123-9.
 130. Osawa, T., et al., *Lysyl oxidase secreted by tumor endothelial cells promotes angiogenesis and metastasis*. Br J Cancer, 2013. **109**(8): p. 2237-47.
 131. Liu, J., et al., *Correlations of lysyl oxidase with MMP2/MMP9 expression and its prognostic value in non-small cell lung cancer*. Int J Clin Exp Pathol, 2014. **7**(9): p. 6040-7.
 132. Zeltz, C., et al., *LOXL1 Is Regulated by Integrin alpha11 and Promotes Non-Small Cell Lung Cancer Tumorigenicity*. Cancers (Basel), 2019. **11**(5).
 133. Peng, D.H., et al., *ZEB1 induces LOXL2-mediated collagen stabilization and*

- deposition in the extracellular matrix to drive lung cancer invasion and metastasis.* *Oncogene*, 2017. **36**(14): p. 1925-1938.
134. Mahjour, F., et al., *Mechanism for oral tumor cell lysyl oxidase like-2 in cancer development: synergy with PDGF-AB.* *Oncogenesis*, 2019. **8**(5): p. 34.
 135. Miller, B.W., et al., *Targeting the LOX/hypoxia axis reverses many of the features that make pancreatic cancer deadly: inhibition of LOX abrogates metastasis and enhances drug efficacy.* *EMBO Mol Med*, 2015. **7**(8): p. 1063-76.
 136. Le Calve, B., et al., *Lysyl oxidase family activity promotes resistance of pancreatic ductal adenocarcinoma to chemotherapy by limiting the intratumoral anticancer drug distribution.* *Oncotarget*, 2016. **7**(22): p. 32100-12.
 137. Ferreira, S., et al., *LOXL2 Inhibitors and Breast Cancer Progression.* *Antioxidants (Basel)*, 2021. **10**(2).
 138. Papadantonakis, N., S. Matsuura, and K. Ravid, *Megakaryocyte pathology and bone marrow fibrosis: the lysyl oxidase connection.* *Blood*, 2012. **120**(9): p. 1774-81.
 139. Siruguri, V., *Journey from food toxins to food safety: Transition over a century in service of nation.* *Indian J Med Res*, 2018. **148**(5): p. 488-495.
 140. Wang, Y., et al., *Animal Models, Pathogenesis, and Potential Treatment of Thoracic Aortic Aneurysm.* *Int J Mol Sci*, 2024. **25**(2).
 141. Robson, W.J., *Alcohol misuse.* *Arch Dis Child*, 2001. **84**(2): p. 95-7.
 142. Dolgin, E., *Venerable brain-cancer cell line faces identity crisis.* *Nature*, 2016. **537**(7619): p. 149-50.
 143. Jadus, M.R., et al., *Human U251MG glioma cells expressing the membrane form of macrophage colony-stimulating factor (mM-CSF) are killed by human monocytes in vitro and are rejected within immunodeficient mice via paraptosis that is associated with increased expression of three different heat shock proteins.* *Cancer Gene Ther*, 2003. **10**(5): p. 411-20.
 144. Stein, G.H., *T98G: an anchorage-independent human tumor cell line that*

- exhibits stationary phase G1 arrest in vitro.* J Cell Physiol, 1979. **99**(1): p. 43-54.
145. Furnari, F.B., et al., *Malignant astrocytic glioma: genetics, biology, and paths to treatment.* Genes Dev, 2007. **21**(21): p. 2683-710.
146. Alcantara Llaguno, S., et al., *Malignant astrocytomas originate from neural stem/progenitor cells in a somatic tumor suppressor mouse model.* Cancer Cell, 2009. **15**(1): p. 45-56.
147. Cancer Genome Atlas Research, N., *Comprehensive genomic characterization defines human glioblastoma genes and core pathways.* Nature, 2008. **455**(7216): p. 1061-8.
148. Kwon, C.H., et al., *Pten haploinsufficiency accelerates formation of high-grade astrocytomas.* Cancer Res, 2008. **68**(9): p. 3286-94.
149. Zhu, Y., et al., *Early inactivation of p53 tumor suppressor gene cooperating with NF1 loss induces malignant astrocytoma.* Cancer Cell, 2005. **8**(2): p. 119-30.
150. Alvarez-Buylla, A. and D.A. Lim, *For the long run: maintaining germinal niches in the adult brain.* Neuron, 2004. **41**(5): p. 683-6.
151. Susaki, E.A., et al., *Whole-brain imaging with single-cell resolution using chemical cocktails and computational analysis.* Cell, 2014. **157**(3): p. 726-39.
152. Molinaro, A.M., et al., *Genetic and molecular epidemiology of adult diffuse glioma.* Nat Rev Neurol, 2019. **15**(7): p. 405-417.
153. Aldape, K., et al., *Glioblastoma: pathology, molecular mechanisms and markers.* Acta Neuropathol, 2015. **129**(6): p. 829-48.
154. Gong, A.H., et al., *FoxM1 Drives a Feed-Forward STAT3-Activation Signaling Loop That Promotes the Self-Renewal and Tumorigenicity of Glioblastoma Stem-like Cells.* Cancer Res, 2015. **75**(11): p. 2337-48.
155. Uhrbom, L., et al., *Induction of brain tumors in mice using a recombinant platelet-derived growth factor B-chain retrovirus.* Cancer Res, 1998. **58**(23): p. 5275-9.
156. Uhrbom, L., et al., *Dependence of autocrine growth factor stimulation in*

- platelet-derived growth factor-B-induced mouse brain tumor cells*. Int J Cancer, 2000. **85**(3): p. 398-406.
157. Heldin, C.H., *Targeting the PDGF signaling pathway in tumor treatment*. Cell Commun Signal, 2013. **11**: p. 97.
158. Miller, C.R. and A.B. Hjelmeland, *Breaking the feed forward inflammatory cytokine loop in the tumor microenvironment of PDGFB-driven glioblastomas*. J Clin Invest, 2023. **133**(22).
159. Zhou, W., et al., *Targeting Glioma Stem Cell-Derived Pericytes Disrupts the Blood-Tumor Barrier and Improves Chemotherapeutic Efficacy*. Cell Stem Cell, 2017. **21**(5): p. 591-603 e4.
160. Franco, M., et al., *Pericytes promote endothelial cell survival through induction of autocrine VEGF-A signaling and Bcl-w expression*. Blood, 2011. **118**(10): p. 2906-17.
161. Takei, N., I. Nihonmatsu, and H. Kawamura, *Age-related decline of acetylcholine release evoked by depolarizing stimulation*. Neurosci Lett, 1989. **101**(2): p. 182-6.
162. Carmeliet, P. and R.K. Jain, *Principles and mechanisms of vessel normalization for cancer and other angiogenic diseases*. Nat Rev Drug Discov, 2011. **10**(6): p. 417-27.
163. Bergers, G., et al., *Benefits of targeting both pericytes and endothelial cells in the tumor vasculature with kinase inhibitors*. J Clin Invest, 2003. **111**(9): p. 1287-95.
164. Zudaire, E., et al., *A computational tool for quantitative analysis of vascular networks*. PLoS One, 2011. **6**(11): p. e27385.
165. Govindaraj, I., et al., *Quantification of vascular changes in macular telangiectasia type 2 with AngioTool software*. Graefes Arch Clin Exp Ophthalmol, 2024.
166. Gustavsson, S.T., et al., *Nicotinamide Prevents Retinal Vascular Dropout in a Rat Model of Ocular Hypertension and Supports Ocular Blood Supply in Glaucoma Patients*. Invest Ophthalmol Vis Sci, 2023. **64**(14): p. 34.

167. Peng, K., et al., *HIF-1alpha promotes kidney organoid vascularization and applications in disease modeling*. Stem Cell Res Ther, 2023. **14**(1): p. 336.
168. Lee, M., et al., *Retinal hypoxia and angiogenesis with methamphetamine*. Exp Eye Res, 2021. **206**: p. 108540.
169. Abramsson, A., P. Lindblom, and C. Betsholtz, *Endothelial and nonendothelial sources of PDGF-B regulate pericyte recruitment and influence vascular pattern formation in tumors*. J Clin Invest, 2003. **112**(8): p. 1142-51.
170. Nitzsche, B., et al., *Coalescent angiogenesis-evidence for a novel concept of vascular network maturation*. Angiogenesis, 2022. **25**(1): p. 35-45.
171. Birzu, C., et al., *Recurrent Glioblastoma: From Molecular Landscape to New Treatment Perspectives*. Cancers (Basel), 2020. **13**(1).
172. Cribaro, G.P., et al., *Three-dimensional vascular microenvironment landscape in human glioblastoma*. Acta Neuropathol Commun, 2021. **9**(1): p. 24.
173. Friedman, H.S., et al., *Bevacizumab alone and in combination with irinotecan in recurrent glioblastoma*. J Clin Oncol, 2009. **27**(28): p. 4733-40.
174. Gilbert, M.R., et al., *A randomized trial of bevacizumab for newly diagnosed glioblastoma*. N Engl J Med, 2014. **370**(8): p. 699-708.
175. Reardon, D.A., et al., *A review of VEGF/VEGFR-targeted therapeutics for recurrent glioblastoma*. J Natl Compr Canc Netw, 2011. **9**(4): p. 414-27.
176. Bondareva, A., et al., *The lysyl oxidase inhibitor, beta-aminopropionitrile, diminishes the metastatic colonization potential of circulating breast cancer cells*. PLoS One, 2009. **4**(5): p. e5620.
177. **Gen Li**, Jerry Voncken, Huabin Zhang, Dongxu Zhao, Roland E. Kälin and Rainer Glass. *Tracing pericyte heterogeneity in the glioblastoma vasculature*. Poster, Brain Tumor Meeting 2024, Berlin, Germany.
178. Zhao D, et al., *Comparing Tumor Cell Invasion and Myeloid Cell Composition in Compatible Primary and Relapsing Glioblastoma*. Cancers (Basel). 2021 Jul 20;13(14):3636.

Contributions

I hereby declare that the animal model induction and cell culture for this research were primarily conducted by myself, with valuable assistance from other lab members, including Mr. Jerry Voncken, Mr. Ding Zhou, and Mr. Wangyang Song. The cell transduction was performed by PD Dr. Roland E. Kälin, a postdoctoral researcher in our lab and my co-supervisor. All other experimental procedures and analyses were carried out independently by me, under the supervision of my supervisor Prof. Dr. Rainer Glass, with guidance from my thesis advisory committee members, Prof. Dr. Wolfgang Enard and Prof. Dr. Christian Schulz. All written content was composed solely by me.

Acknowledgement

My first deep gratitude goes to my supervisor Prof. Dr. Rainer Glass. I am grateful that he gave me the precious chance to work in his lab where I accepted strict scientific practice. I also thank his continuous and extraordinary help in all stages of my Dr. med studies. His profound knowledge, serious research attitude and rigorous thinking made me benefit a lot from him. Besides, I want to give my gratitude to my co-supervisors, Prof. Dr. Wolfgang Enard and Prof. Dr. Christian Schulz for their advice, helped to improve my research and presentation skills.

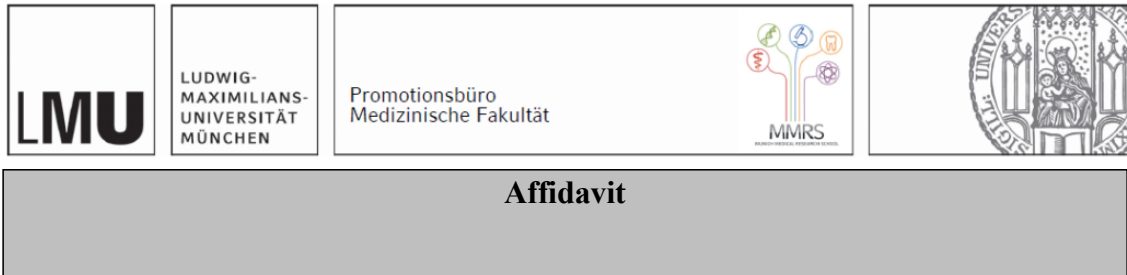
I want to thank Dr. Roland Kaelin for his suggestions and assistance with my research. His comments and advice on my experiments always give me new thoughts on how to solve my problems. I am particularly grateful to Ms. Stefanie Lange, not only for her technical support, but also her generous help with problems of my daily life.

Moreover, my great thanks go to other members of neurosurgical research group. I am grateful Dr. Zhang Huabin and Dr. Zhao Dongxu gave me their great help at the beginning of my lab life in Germany. I thank Dr. Cheng Jiying for her generous help with my research, also for the happy days we had together in Germany. I thank Mr. Song Wangyang, a great scientist, also my good friend for our precious time. I thank Mr. Zhu Sihan for his kind help with my personal issue after I left Germany, also for the beautiful time we spent together in Europe. I also want to thank Mr. Ding Zhou, Mr. Enio Barci, Mr. Jerry Voncken and all other lab colleagues, for their accompany and help. I would also express my gratitude to Dr. Steffen Dietzel, Dr. Andreas Thomae and Dr. Mariano Pisfil for their technical support with imaging process. Besides, I want to thank all my friends in Munich.

I am also grateful for the kind financial support from China Scholarship Council (CSC).

Last but not least, I want to thank my family, especially my wife Zhao Lei, for supporting me to chase my dream, to finish my doctoral research in Germany, a country that far away from my home. My wife, my parents and grandparents gave me lots of courage which is of great importance for me to go through all the difficulties.

Affidavit



Li, Gen

Surname, first name

I hereby declare, that the submitted thesis entitled:

Investigating Pericyte heterogeneity in the glioblastoma vasculature

is my own work. I have only used the sources indicated and have not made unauthorised use of services of a third party. Where the work of others has been quoted or reproduced, the source is always given.

I further declare that the dissertation presented here has not been submitted in the same or similar form to any other institution for the purpose of obtaining an academic degree.

Zhengzhou 24.04.2025

place,date

Gen Li

Signature doctoral candidate

List of Publications

1. Cheng J, Li M, Motta E, Barci D, Song W, Zhou D, **Li G**, Zhu S, Yang A, Vaillant BD, Imhof A, Forné I, Spiegl-Kreinecker S, Zhang N, Katayama H, Bhat KPL, Flüh C, Kälin RE, Glass R. Myeloid cells coordinately induce glioma cell-intrinsic and cell-extrinsic pathways for chemoresistance via GP130 signaling. *Cell Rep Med*. 2024 Aug 20;5(8):101658.
2. **Gen Li***, Yushu Dong*, Dongdong Liu, Zheng Zou, Guangzhi Hao, Xu Gao, Pengyu Pan*, Guobiao Liang*, NEK7 Coordinates Rapid Neuroinflammation After Subarachnoid Hemorrhage in Mice, *Frontiers in Neurology*, 2020 Jul 8;11:551.
3. Dongdong Liu*, Yushu Dong*, **Gen Li**, Zheng Zou, Guangzhi Hao, Hua Feng, Pengyu Pan*, Guobiao Liang*, Melatonin Attenuate White Matter Injury via Reducing Oligodendrocyte Apoptosis After Subarachnoid Hemorrhage in Mice, *Turkish Neurosurgery*, Jan 22.
4. Dongdong Liu, Zheng Zou, **Gen Li**, Pengyu Pan, Guobiao Liang, Long Noncoding RNA NEAT1 Suppresses Proliferation and Promotes Apoptosis of Glioma Cells Via Downregulating MiR-92b, *Cancer Control*, Jan-Dec 2020;27(1):1073274819897977.
5. Zheng Zou*, Yushu Dong, Dongdong Liu, **Gen Li**, Guangzhi Hao, Xu Gao, Pengyu Pan*, Guobiao Liang*, MAP4K4 Induces Early Blood-brain Barrier Damage in a Murine Subarachnoid Hemorrhage Model, *Neural Regeneration Research*, 2021 Feb;16(2):325-332.